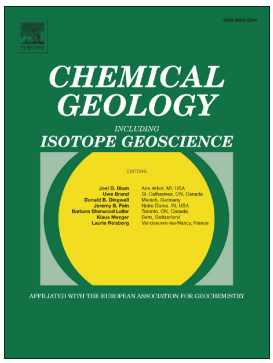

Rare earth elements and radiogenic strontium isotopes in carbonate minerals reveal diagenetic influence in shales and limestones in the Appalachian Basin

Thai T. Phan, J. Alexandra Hakala, Christina L. Lopano, Shikha Sharma

PII: S0009-2541(19)30034-8
DOI: https://doi.org/10.1016/j.chemgeo.2019.01.018
Reference: CHEMGE 19046

To appear in: *Chemical Geology*

Received date: 12 October 2018
Revised date: 9 January 2019
Accepted date: 26 January 2019

Please cite this article as: T.T. Phan, J.A. Hakala, C.L. Lopano, et al., Rare earth elements and radiogenic strontium isotopes in carbonate minerals reveal diagenetic influence in shales and limestones in the Appalachian Basin, Chemical Geology, https://doi.org/10.1016/j.chemgeo.2019.01.018

Rare earth elements and radiogenic strontium isotopes in carbonate minerals reveal diagenetic influence in shales and limestones in the Appalachian Basin

Thai T. Phan[a-c*], J. Alexandra Hakala[a], Christina L. Lopano[a], Shikha Sharma[d]

[a]National Energy Technology Laboratory, U.S. Department of Energy, Pittsburgh, PA 15236, USA
[b]Department of Geology and Environmental Science, University of Pittsburgh, Pittsburgh, PA, 15260, USA
[c]Department of Earth and Environmental Sciences, University of Waterloo, Waterloo, ON N2L 3G1, Canada
[d]Department of Geology and Geography, West Virginia University, Morgantown, WV 26506, USA

[*]Corresponding author:

Thai T. Phan
Department of Earth and Environmental Sciences, University of Waterloo
200 University Ave. W, Ontario, N2L 3G1, Canada
Email: thai.phan@uwaterloo.ca

Abstract

Rare earth element (REE) signatures are often applied to interpret paleoenvironmental conditions in sedimentary basins, however the complicated diagenetic histories in dynamic depositional environments can affect interpretation of measured REE signatures. Prior studies on REE content in shales and limestones indicated that REE in specific mineral phases may provide unique information concerning diagenetic reactions occurring in sedimentary rocks during burial and compaction. Application of sequential extraction techniques to target REE signatures in specific mineral fractions may provide greater insight into the complex processes that occurred during diagenesis and catagenesis. Thus, using this technique, this study provides a detailed account for REE, $^{87}Sr/^{86}Sr$, and $\delta^{13}C$ in the carbonate fraction of the Marcellus Shale and adjacent formations in the Appalachian Basin. A suite of 49 rock samples collected from two cores recovered from Monongalia County, West Virginia, USA was analyzed. The results showed that the carbonate concretions in calcareous shales and carbonate cements in black shales were very distinct. The REE plus yttrium (REY) were more concentrated in the carbonate concretions than in the carbonate cements. The carbonate concretions displayed REY patterns that are closely similar to modern seawater, while MREE-enrichment was observed in the carbonate cements. Likewise, the $^{87}Sr/^{86}Sr$ values in the carbonate concretions were similar to those measured for unaltered Middle Devonian carbonates, while the $^{87}Sr/^{86}Sr$ in the carbonate cements were much more radiogenic. This observation indicates that the carbonate cement could have been inherited radiogenic ^{87}Sr expulsed from clays during illite-smectite transition. Overall, this study demonstrated two distinct processes involved with controlling the carbonate geochemistry within Appalachian Basin shales and limestones: one fraction displaying minimal diagenetic alteration relative to depositional conditions (carbonate concretions in calcareous shales and limestone carbonate in limestones), and another fraction displaying the evidence for extensive chemical alteration during illite-smectite transition and catagenesis (carbonate cements in black shales). In addition, highly variable and significant enrichments of U and Mo demonstrate that the Union Spring member and the Lower Oatka Creek member of the Marcellus Shale in the southwestern Appalachian Basin (MSEEL site) were deposited under mainly anoxic environment whereas intermitted episodes of dysoxic to perhaps oxic conditions occurred during the deposition of the Upper Oatka Creek member.

Key words

Rare earth elements; diagenesis; paleoenvironment; carbonates; middle REE enrichment; sequential extractions; black shales; Marcellus Shale; illite-smectite transition; radiogenic strontium isotopes

1 Introduction

Understanding the origin of petroleum source rocks assists in development of unconventional resource plays, which have proven to be successful sources of oil and gas worldwide (Tissot and Welte, 2012). Historical characterization of kerogen thermal maturation has largely relied on inferences from data collected from conventional reservoirs and may not provide the best information on the diagenetic and catagenetic processes affecting kerogen structure and hydrocarbon generation (Agarwal and Sharma, 2018a, b). An ability to characterize the depositional and diagenetic history of unconventional reservoirs can lead to improved stimulation design and increases in overall oil and gas production.

Characterizing the extent to which shale has undergone catagenesis can be of value in determining the type of hydrocarbon produced and its overall for hydrocarbon generating potential in unconventional reservoirs. Mineralization of organic matter into carbonate minerals can provide key information on thermal maturity, hydrocarbon prospectivity and flow path. Geochemical tracers present in different fractions of reservoir rock, including both carbonate and clay phases, can be used to characterize the depositional and diagenetic history of subsurface reservoirs (Phan et al., 2016; Williams et al., 2013). Prior studies have demonstrated the utility of rare earth elements (REE), $^{87}Sr/^{86}Sr$, and $\delta^{13}C$ in both carbonate and clay phases as useful indicators for characterizing diagenetic processes (Chaudhuri and Clauer, 1993; Chen and Sharma, 2016; Osborn et al., 2012; Phan et al., 2018b; Stewart et al., 2015).

The concentration and distribution of rare earth elements (REE) can be applied towards characterizing important diagenetic and catagenetic processes in shale (e.g., Phan et al., 2018b). For example, the post Archean Australian Shale (PAAS) normalized REE in black shales, that are primarily sourced from detrital siliciclastics, mostly display flat patterns (Phan et al., 2018b; Yang et al., 2017). Shales containing authigenic components can display more variable whole-rock REE patterns if there is a significant contribution of REE from the authigenic components to the bulk REE inventory (this study; Yang et al., 2017). Authigenic alterations may not always be observed in whole rock REE data due to a less significant contribution of REE from authigenic phases, or due to contrasting influences of REE signatures from different mineral fractions within a sample. For example, middle REE enriched patterns were observed in separated conodont apatite, but not in the whole rock REE signature, of Huanghuachang and

Chenjiahe samples (Hubei Province, South China; Zhang et al., 2016). Sequentially-extracted fractions from Marcellus Shale (Greene county, PA, USA) reflect mineralogy-specific post-depositional changes compared to the primary REE pattern associated with silicate minerals in the shale (Phan et al., 2018b). Both $^{87}Sr/^{86}Sr$ and $\delta^{13}C$ measurements in have been applied to confirm detrital versus seawater-derived influences on depositional and diagenetic history in Marcellus Shale (Phan et al., 2018b; Chen and Sharma, 2017). Targeted analysis of REEs, $^{87}Sr/^{86}Sr$ and $\delta^{13}C$ of dissolved inorganic carbon ($\delta^{13}C$-DIC) in sequentially extracted fractions of shales can provide detailed information on the post-depositional processes affecting the shale.

Black shales like the Marcellus Shale are silt-bearing mudstones (Macquaker and Adams, 2003) composed primarily of siliciclastic debris including illitic clay, quartz, and feldspars and authigenic components, such as marine derived organic matter, carbonate cement, pyrite, and barite (this study; Chen and Sharma, 2016; Milliken et al., 2013; Niu et al., 2016; Phan et al., 2018b; Sageman et al., 2003; Werne et al., 2002). Previous studies showed that the carbonate cement in the Marcellus Shale is of diagenetic origin and not representative of Middle Devonian seawater (Lash and Blood, 2014; Chen and Sharma, 2017; Phan et al., 2018b) whereas carbonate minerals in adjacent limestone units are likely derived from direct precipitation from Middle Devonian seawater (Phan et al., 2018b).

We hypothesize that different authigenic components in shales, mainly carbonate cements and clays, can provide a record of diagenetic alterations during catagenesis. Therefore, in this study, we characterized both whole rock and authigenic components of Marcellus Shale, carbonate-rich concretions within the shale, and limestones from the Appalachian Basin. High resolution analysis of REE and yttrium (REY), $^{87}Sr/^{86}Sr$, and $\delta^{13}C$-DIC was conducted along a 30 m (100 ft) Marcellus Shale core to perform a robust evaluation of the degree of diagenetic influence across the stratigraphic depth. In addition, the enrichment factors of U and Mo were used to investigate the differences in the depositional environment at the study area compared to other regions of the Appalachian Basin. To our knowledge, this is the first study to present high-resolution, phase-specific data to characterize catagenesis in the Marcellus Shale.

2 Methods

2.1 Study area and samples

The high-resolution analysis in this study primarily focuses on the Marcellus Shale in Monongalia County, West Virginia, USA. In this location, the Marcellus Shale is approximately 30 m thick and divided into three members. The Upper and Lower Oatka Creek members in the uppermost portion of the Marcellus Shale are separated from the Union Springs member by the Cherry Valley limestone formation at about 2292 m depth. The Union Springs member is in the lowermost portion of the Marcellus Shale where horizontal drilling for hydraulic fracturing usually occurs. For comparison to other stratigraphic units, the Mahantango Shale, Burket (Geneseo) Shale and Tully Limestone were analyzed as part of this study. The Burket (Geneseo) is a black organic-rich shale that lies immediately on top of the Tully Limestone and is an Upper Devonian formation. Geneseo refers to the portion in northeastern Pennsylvania and southern New York whereas the formation is referred to as Burket in our study area (West Virginia) and most parts of Pennsylvania. In contrast to Burket Shale, Mahantango Shale is a gray/brown organic poor shale, typically found conformally overlying the Marcellus Shale.

A suite of 49 rock samples were collected from two well cores recovered from the Marcellus Shale Energy and Environment Laboratory (MSEEL) field site in Monongalia County, WV, USA (filled circle, **Fig. 1**). Samples from the first drill core (MIP-3H, 39°36'06.5"N 79°58'34.0"W) cover both Oatka Creek and Union Springs members of the Marcellus Shale whereas samples of adjacent formations: Burket (Geneseo) Shale, Tully Limestone, Mahantango Shale were collected from side wall sub-cores of the second well (MIP-SW, 39°36'32.0"N 79°58'47.7"W). The two samples from TG site in Tioga County, PA, USA were from an undisclosed well location.

Five different macro-facies units are present in Marcellus Shale: 1) organic siliceous shale; 2) organic mudstone; 3) organic mixed shale; 4) gray siliceous shale, and; 5) gray mixed shale and gray mudstone in which these macro-facies units are lensed with carbonate layers (Paronish, 2018). Additional details of the macro-facies analysis of these two cores can be found in Paronish (2018). Our study refers to clay and quartz-rich samples with carbonate content <10% and >10% as shale and calcareous shale, respectively. Rock samples that are poor in quartz and clays with carbonate content >40% are referred to as limestone. All rock samples were

pulverized using a mixer mill and then divided into desired weights by a splitter. Pulverized rock samples were digested by fusion and then further digested by acids for bulk concentrations of both major and trace elements including REY.

2.2 Bulk rock digestion and sequential extraction methods

Because REY associated with non-carbonate minerals (e.g., Fe–Mn oxyhydroxides, phosphates, clays, and adsorbed on organic matter and clays,) can potentially conceal the original REY signature of carbonate minerals (Phan et al., 2018b; Zhang et al., 2015), a sequential extraction procedure, previously applied on limestones and shales (Phan et al., 2015; Phan et al., 2018b), was applied on samples in this study (Procedure A in **Fig. 2**). Briefly, about 1 g split of rock powder was sequentially leached to extract water-soluble salts (water-soluble fraction) using Milli-Q water. The residue was further treated with 1.0 N ammonium acetate pH 8 to extract adsorbed metals (exchangeable fraction), and the desorption process is quick in high ionic strength solution (Willis and Johannesson, 2011). For example, it takes less than 5 minutes to desorb REE from natural clays (Moldoveanu and Papangelakis, 2012). Next, the residue was treated with 1.0 N acetic acid for 4 hours to primarily dissolve calcite and dolomites (major carbonate fraction), and potentially authigenic carbonate fluorapatite if present. Phan et al. (2018b) found that less than 0.2% of Al was dissolved in this fraction, suggesting that the dissolution of aluminosilicate minerals exhibited minimal influence on the carbonate REY patterns. We monitored Al in these leachates to evaluate if carbonate REY is influenced by preferential leaching of clays. The residues of select samples of the Marcellus Shale were further treated with 1.0 N acetic acid for an additional 2 hours to dissolve the remaining carbonates (remaining carbonate fraction).

Procedure B (**Fig. 2**) was similar to procedure A, except that diluted nitric acid (0.2 N HNO_3) was used for 15 minutes to partially dissolve carbonate minerals (Tostevin et al., 2016). Due to the difference in carbonate content, we used slightly different procedures for limestone and shale: 10 mL 0.2N HNO_3 per gram of limestone samples whereas 5 mL 0.2 N HNO_3 per gram of shale was used. The REY and trace metal concentration data of the three carbonate fractions: 1.0 N acetic acid (4 hours), 1.0 N acetic acid (additional 2 hours), and 0.2 N HNO_3 (15 minutes) were compared to evaluate the efficacy of each leaching procedure in obtaining the original carbonate REY patterns.

An adaptation of the Soxhlet extraction method using organic solvents (Wei et al., 2014), was used to extract REY associated with organic matter in select shale samples (Procedure C in **Fig. 2**). The extraction process was conducted in 50 mL centrifuge tubes (polypropylene) placed inside a Teflon coated rack on a hot plate to allow for high throughout sample processing. According to Wei et al., (2014), dichloromethane mostly extracts long-chained and unbranched aliphatics whereas toluene dissolves short-chained and highly branched aliphatics. All leachates were centrifuged, and supernatants were syringe-filtered through 0.2 µm membrane to avoid fine clays passing through the membrane (Phan et al., 2018a). Organic solvent leachates from procedure C were further digested by aqua regia, and then treated with concentrated H_2O_2 until no visible dark brown residue was observed. For the water-soluble leachates, an aliquot was taken and immediately refrigerated for ion chromatography analysis on the next day, and the remaining aliquot was acidified with HNO_3. All other leachates were evaporated to dryness and further treated with 10 drops of concentrated HNO_3 and 10 drops of concentrated H_2O_2. The residues were re-dissolved in 2% HNO_3 prior to analysis. All reagents used in this study were ultrapure grade (Optima^{TM} grade, Fisher Chemical) and lab wares were acid washed prior to use.

2.3 Analytical techniques

Mineral and organic content of the samples were analyzed via XRD and CHNS Elemental Analysis. Pulverized rock samples were back-loaded into a cavity mount spinning holder and scanned by a PanAlytical X'Pert Pro X-ray diffractometer (XRD) equipped with Cu radiation at the National Energy Technology Laboratory (NETL) in Pittsburgh, PA, USA. The reported percentages of mineral composition (**Table 1**) were semi-quantitatively estimated using the reference-intensity ratio matrix-flushing method (Chung, 1974) and the mineral percentages were then corrected for the total organic carbon (TOC) content of bulk rocks (100%-%TOC). The TOC was analyzed at the NETL by CHNS Elemental Analyzers. Select samples were analyzed at the IsoBioGem Laboratory at West Virginia University, WV, USA.

Major elements, trace, and REY were analyzed on a PerkinElmer NexION 300X ICP-MS using kinetic energy discrimination (KED) mode at the University of Pittsburgh whereas major and minor metal concentrations of bulk rocks were measured at the NETL Pittsburgh Analytical Laboratory using fusion method, and then analyzed on a PerkinElmer NexION 300X ICP-MS. Oxide interference on REY (Dulski, 1994)) was monitored using formation rate of Ce and Co

oxides (CeO/Ce <0.003; CoO/Co <0.003). During analysis, single element Ba (2000 µg/L) solution was analyzed to evaluate the polyatomic interference on REY. This Ba solution always yielded Ce less than 0.002 µg/L which is negligible relative to measured concentrations of REY (>0.5 µg/L). For REY with multiple isotopes, measured concentrations of each isotope of the same element are within 5%; thus, the average concentration (Phan et al., 2018b) was reported. The estimated accuracy of both major and trace elements including REY was better than 10% (within 20% for Dy and Er) based on replicate measurements of the USGS rock standards: SGR-1b (shale) and SBC-1 (shale); and freshwater standards: T-227 (spring water; USGS), NIST-1640a (spring water; NIST). The method detection limit was defined based on 3 standard deviations of replicate measurements of T-227. The procedural blanks of the sequential leaching procedure were below the limits of detection.

The REY patterns were plotted by normalizing the REY concentrations to chondrite and PAAS. The REY data of chondrite and PAAS used in this study are from Pourmand et al. (2012). To facilitate the comparison of the REY patterns, the bell-shaped index (BSI) was calculated using the equation (Tostevin et al., 2016) below and used to approximate the enrichment of the MREE (**Eq. 1**).

$$\mathrm{BSI} = \frac{2([\mathrm{Sm}]_{\mathrm{SN}}+[\mathrm{Gd}]_{\mathrm{SN}}+[\mathrm{Dy}]_{\mathrm{SN}})/3}{([\mathrm{La}]_{\mathrm{SN}}+[\mathrm{Pr}]_{\mathrm{SN}}+[\mathrm{Nd}]_{\mathrm{SN}})/3+([\mathrm{Ho}]_{\mathrm{SN}}+[\mathrm{Er}]_{\mathrm{SN}}+[\mathrm{Tm}]_{\mathrm{SN}}+[\mathrm{Yb}]_{\mathrm{SN}}+[\mathrm{Lu}]_{\mathrm{SN}})/5} \quad (1)$$

where SN denotes shale (PAAS) normalization. The higher value of BSI means the REY pattern exhibits greater enrichment of MREE. In addition, the concentrations of U and Mo in bulk rocks were normalized to Al to minimize the effects of dilution due to the presence of carbonate and biogenic silica (Tribovillard et al., 2006). The enrichment factors (EF) of U and Mo can be defined as:

$$\mathrm{X-EF} = \left(\frac{([\mathrm{X}]/[\mathrm{Al}])_{\mathrm{sample}}}{([\mathrm{X}]/[\mathrm{Al}])_{\mathrm{PAAS}}}\right) \quad (2)$$

where [X] denotes the concentration of the element (**Eq. 2**). The concentrations of these elements of PAAS are from Taylor and McLennan (1985). Previous studies (Algeo and Tribovillard, 2009; Tribovillard et al., 2012) showed that the correlation between U and Mo enrichment in marine sediments could elucidate information regarding redox conditions of bottom water and the operation of metal-oxyhydroxide particulate shuttles. Thus, U-EF and Mo-EF will be used to discuss the redox conditions during the Marcellus Shale deposition.

The C isotopes of the carbonate fraction of select samples were analyzed on a GasBench II device coupled to a Finnigan Delta V Advantage mass spectrometer at the IsoBioGem Laboratory at West Virginia University, WV, USA following the Chen and Sharma (2016) method. The C isotope data are reported as $\delta^{13}C$, per mil deviation from the Vienna PeeDee Belemnite (V-PDB) standard. Typical precision of $\delta^{13}C$ values is better than ±0.1‰ based on replicate analysis of the samples and in-house standards.

Radiogenic Sr isotopes of the leachates were measured by the ThermoFisher Neptune Plus multi-collector inductively coupled plasma mass-spectrometer (MC-ICP-MS) at the University of Pittsburgh, following the Wall et al. (2013) high-throughput method. The measured $^{87}Sr/^{86}Sr$ was normalized to SRM987 Sr standard ($^{87}Sr/^{86}Sr = 0.710240$) to facilitate the comparison with the previously reported data from the lab. In each analytical session, two reference standards were processed together with the samples to ensure the data quality. The measured $^{87}Sr/^{86}Sr$ value of UD6−120518−S (produced water in-house standard) was 0.719957±0.000032 (n=8) which agrees well with 0.719956±0.000041 (2SD; n=8)(Kolesar Kohl et al., 2014; Phan et al., 2016); $^{87}Sr/^{86}Sr = 0.719958±0.000020$ (2SD; n=9)(Phan et al., 2018c). Likewise, analysis of EN−1 (shell of giant clam, USGS) in this study yielded $^{87}Sr/^{86}Sr = 0.709156±0.000048$ (2SD; n=8), consistent with $^{87}Sr/^{86}Sr = 0.709159±0.000032$ (2SD; n=9)(Phan et al., 2018c) and $^{87}Sr/^{86}Sr = 0.709169$ (Neymark et al., 2014), where their measured $^{87}Sr/^{86}Sr$ is normalized to 0.710240.

3 Results

3.1 Mineralogical compositions of shales and limestones from Appalachian Basin

Marcellus Shale samples all are rich in quartz (29-44%) and clays (31-57%) (**Table 1**). Muscovite and illite (30-48%) are found in all samples of Oatka Creek and Union Springs members whereas chlorite is only found in the Oatka Creek members (8-10%). Carbonates (calcite and dolomite) in shales range from 1% to 21%, in which calcite is more dominant than dolomite. Pyrite (up to ~ 5%) is present in all samples. Barite (~ 3%) was detected in one out of ten analyzed samples. Albite (8%) is present in two samples from Tioga County, PA, but not observed in the samples from Monongalia County, WV. No soluble salts such as halite were detected. Burket and Mahantango shales are also rich in quartz and clays (muscovite/illite and chlorite), however, very poor in carbonates (not detected).

Carbonate contents of the Marcellus Shale range from <0.5% to as much as 26% (**Fig. 3**A) whereas carbonate contents of Burket and Mahantango shales are very low, <0.5% and <1.5%, respectively (**Table 2**). The carbonate contents (weight % as $CaCO_3$ and $MgCO_3$) reported in **Table 2** are calculated based on the concentrations of Ca and Mg extracted in the 1.0 N acetic acid leachates, following the convention used in Phan et al., (2015). The carbonate content of Cherry Valley limestone (located within the Marcellus Shale, e.g. **Fig. 1**) and Tully limestone range from 47 to 73% (**Table 2**).

Organic poor shales (TOC<5%) are found in the uppermost portion, whereas organic-rich shales (TOC>5%) are in the lowermost portion, of the Marcellus Shale (**Table 2; Fig. 3**B). The TOC of Cherry Valley limestone (2%) is much lower than the adjacent organic-rich zones comprising the Union Springs member and part of the Lower Oatka Creek member. In the Union Springs member, the TOC increases with depth ranging from 4.5% to 12%. The Marcellus Shale gamma-ray signature preserved in the MIP-3H core is mimicked by the TOC profile. The TOC of Burket shale ranges from 5 to 7% (**Table 2**).

Based on these results, in this study, we will refer to clay and quartz-rich samples with carbonate content <10% and >10% as shale and calcareous shale, respectively. Rock samples that are poor in quartz and clays with carbonate content >40% are referred to as limestone.

3.2 Whole-rock geochemical proxies and REY

3.2.1 Whole-rock major elemental compositions

The TiO_2, Al_2O_3, and SiO_2 contents of MIP-3H core exhibit a step-wise increase upward from Union Springs at the base to Upper Oatka Creek member at the top of the Marcellus Shale (**Fig. 3**). Strong correlation (r^2=0.93; n=33) between TiO_2 and Al_2O_3 is observed for all samples (shale, calcareous shale, and limestone) from the MIP-3H core. Like TOC, the Si/Al ratios generally increase with sample depths (higher Si/Al ratios are found in deeper shale samples) in the Union Springs member (**Fig. 4**). The Si/Al ratios in the Union Springs member are much higher than those in the Oatka Creek members where Si/Al mostly remain constant with depth (**Fig. 4**A). At the base of the Union Springs member, Fe/Al ratios are greater than 1 (1.1 – 1.8) whereas Fe/Al ratios in the upper portions (<2298 m) are generally <0.5 and do not change with depth (**Fig. 4**B). Similar Fe/Al ratios are observed in shales of the Burket Shale and Mahantango Shale

(**Table 2**). The Fe/Al of limestones are generally greater than Fe/Al of shales, probably due to low clastic input (**Table 2**).

Bulk P contents do not vary with depth (**Fig. 5**A) except two Marcellus Shale samples (MIP-3H) containing higher levels of P (>1000 ppm): one black shale sample in the Upper Oatka Creek member and one limestone sample in the Union Springs member. In addition, P in one Marcellus Shale sample of Union Springs member from MIP-SW core (SW-5; **Table 2**) is 1380 ppm which is also greater than most of the shale samples (450 ± 250 ppm; 2SD; n=44) reported in this study.

3.2.2 Whole-rock enrichment factors of U and Mo

For black and calcareous shales of the Marcellus Shale (MIP-3H core; n=33), the depth profiles of U (3 – 75 ppm) and Mo (2 – 343 ppm) resemble the TOC profile (**Fig. 3**B). The Th/U ratios increase upward from the base to the top of the Marcellus Shale. The highest Th/U is found in a calcareous shale sample (depth = 2272 m; **Fig. 4**C). U concentrations in Burket Shale (16 – 27 ppm) are in similar range with U in the Marcellus Shale, and Mahantango Shale is poor in U (3 – 5 ppm). U in limestones of Cherry Valley and Tully are poor, ranging from 1 to 3 ppm.

The U-EF and Mo-EF do not change much in the organic poor portion of the Marcellus Shale (MIP-3H) and increase sharply downward starting at the base of the Lower Oatka Creek member. This sharp downward increase of U-EF and Mo-EF is more obvious in a 5 m thick interval (2295 – 2300 m) of the Union Springs (**Fig. 4**D and E). We found that U concentrations correlate well with TOC (r^2=0.79; not shown) and U-EF (r^2=0.86; not shown). Likewise, there is a good correlation between U-EF and Mo-EF (r^2=0.73; not shown).

3.2.3 Whole-rock REY signatures

The total REY (ΣREY; La through Lu and Y) of all shales is in similar range (132 – 402 ppm; n=33) and is generally higher than ΣREY of limestones (85 – 149 ppm; n=5) (**Tables 2 and S1**). A general trend of increasing ΣREY from the basal portion of the Marcellus Shale to the top (**Fig. 5**B) coincides with the trend of increasing Al and Ti contents. When normalized to Al, most shale and limestone samples (~80% of the samples from MIP-3H core) fall on a vertical line (ΣREY/Al = 0.0025±0.0006; 2SD; n=28) (**Figure 5**C). However, the rest of the samples display ΣREY/Al ratios greater than 0.0025. Particularly, four calcareous shales and one P-rich

black shale samples of the Marcellus Shale display anomalously high ΣREY/Al ratios (>0.005) and high ΣREY (>300 ppm; **Fig. 6**). Cross-plots (**Fig. 6**) indicate that the ΣREY of either limestones, calcareous shales, or black shales do not correlate with either carbonate content, P, or TOC, except with Al_2O_3 (r^2=0.52 if excluding the calcareous shales; **Fig. 6**B).

The chondrite-normalized REY patterns of all analyzed shale samples of the Marcellus Shale, Mahantango Shale, and Burket Shale display the enrichment in light REE (LREE, La-Sm) and are relatively flat in heavy REE (HREE, Ho-Lu) (**Fig. 7)**. Chondrite-normalized REY patterns of limestones are similar to the shales, except that limestones display positive Y anomalies (**Fig. 7**B).

Shale and limestone PAAS-normalized REY patterns also are similar (**Fig. 7**B). Most black shales in this study are more concentrated in REY than PAAS (horizontal line), especially calcareous shales, which exhibit large enrichment of the middle REE (MREE, Sm-Dy) and HREE (**Fig. 7**). It is worth noting that the PAAS-normalized REY for black shales are also slightly depleted in light REE (LREE, La-Nd) (**Fig. 7**B). The P-rich black shale sample of the Marcellus Shale shows substantial enrichment in MREE (bell-shaped pattern). Limestones show both Eu and Y positive anomalies whereas these anomalies are not so obvious in calcareous shales and black shales (**Fig. 7**).

3.3 REY signatures in the extracted fractions

A negligible amount <0.2% on average) of REY is extracted in the water-soluble fraction of all analyzed samples. REY adsorbed on the surface of minerals such as clays, and organic matter contributed on average <0.3% of the bulk REY in all rock samples in which adsorbed REY is generally higher in black and calcareous shales than in limestones (**Table S1**). The shale (PAAS) normalized patterns of adsorbed REY are slightly similar to the pattern of modern seawater but depleted in HREE (**Fig. 7**C).

The primary carbonate fractions (extracting using 1.0 N acetic acid for 4 hours) of black shales contain a variable amount of REY (3 – 46 ppm) which contribute anywhere from 1 to 22% of the total REY (**Table S1**). The shale (PAAS) normalized patterns of the primary carbonate in shales used in this study exhibit the enrichment of MREE, typical bell-shaped patterns (**Fig. 7**D**)**. This trend is also observed in the carbonates of the Marcellus Shale from the southcentral (SC site;

Fig. 1) and northeastern (NE site; **Fig. 1**) Appalachian Basin (Phan et al., 2018b). For limestone samples, REY content in the primary carbonate fractions ranges from 57 to 125 ppm which is 41 to 67% of REY of bulk rocks. This is expected because the primary minerals in limestones are calcite and dolomite (**Table 1**). Similarly, carbonates of calcareous shales contain 129 – 219 ppm of REY which contribute 37 – 54% of REY of bulk rocks.

In contrast to carbonate cement in shales, shale normalized REY patterns of the carbonate minerals in limestones and calcareous shales generally exhibit enrichment of HREE relative to LREE, positive Y anomaly, chondritic Y/Ho ratios (31 – 37), and negative Ce anomaly (**Fig. 7**D). These parameters resemble those of modern open seawater (**Fig. 7**C). The BSI of calcareous shales and limestones (<2) are lower than those of carbonate cements in shale (>2) (**Fig. 8**A). For comparison, the BSI of the modern North Atlantic coastal seawater (Tepe and Bau, 2016) and the Middle Devonian Onondaga limestones (Phan et al., 2018b) are 0.75 and 0.99, respectively.

The REY in leachates using dichloromethane and toluene (Procedure C) on select shale samples did not yield measurable REY (**Table S1**; supporting materials).

3.4 Carbon ($\delta^{13}C$) and strontium ($^{87}Sr/^{86}Sr$) isotopes in extracted fractions

The $\delta^{13}C$ in the carbonate fraction across all samples vary over a wide range (ca. -12 – +0.9‰), are lower than $\delta^{13}C$ (ca. 0 – 1‰) of unaltered Middle Devonian carbonates (Saltzman, 2005) which is consistent with $\delta^{13}C$ in the carbonate fraction of Marcellus Shale in SC site (Chen and Sharma 2016). These $\delta^{13}C$ values display no correlation with sample depths (**Fig. 5**D). The $\delta^{13}C$ of Cherry Valley limestone and most of the calcareous shales are lower than the $\delta^{13}C$ of carbonate cement in black shales of the Marcellus Shale (**Fig. 5**D). The $\delta^{13}C$ values of Mahantango Shale and Burket Shale (-5.5 – -2.5‰) are within the range of carbonate cement in the Marcellus Shale. The $\delta^{13}C$ of Tully limestones are -3.0‰ and +0.9‰ which are also lower than the unaltered Middle Devonian carbonates (**Fig. 5**D). The $\delta^{13}C$ was only measured in the carbonate fractions in this study.

The $^{87}Sr/^{86}Sr$ of the exchangeable fraction (adsorbed Sr) of all analyzed rock samples are higher than the $^{87}Sr/^{86}Sr$ of the primary carbonate fraction of the same sample (**Fig. A1**A; supporting materials). This is consistent with a previous study performed on core materials from

southcentral (SC site; **Fig. 1**) and northeastern (NE site; **Fig. 1**) Appalachian Basin (Phan et al., 2018b). For calcareous and black shales of the Marcellus Shale, the $^{87}Sr/^{86}Sr$ values of adsorbed Sr are in similar range (0.7092 – 0.7132) which covers the range of those in Tully Limestones and shales from Mahantango and Burket formations.

The $^{87}Sr/^{86}Sr$ of the primary carbonate fraction of Tully and Cherry Valley limestones and calcareous shales vary in a narrow range (0.7081 – 0.7087) which is close to $^{87}Sr/^{86}Sr$ of unaltered Middle Devonian carbonates (0.7076 – 0.7079; Diener et al., 1996). On the other hand, $^{87}Sr/^{86}Sr$ of the primary carbonate fractions (0.7085 – 0.713) of black shales (i.e., carbonate cement) are much greater (contain more radiogenic isotope) than unaltered Middle Devonian carbonates (**Fig. 8**B). Carbonate cements with high $^{87}Sr/^{86}Sr$ do not necessarily contain higher Sr concentrations, and show no observable difference in Sr/Ca (**Fig. 8**C). For example, the carbonate fractions in the Oatka Creek members are more radiogenic than those in the Union Springs member (**Fig. 5**E).

4 Discussion

4.1 Establishing contributions from carbonate versus detrital minerals in sequentially-extracted fractions

Differentiating contributions from the carbonate and detrital minerals is an important step for ensuring appropriate geochemical interpretations throughout the discussion. Al and $^{87}Sr/^{86}Sr$ signatures can be applied towards evaluating the contributions of carbonate versus detrital minerals to the measured geochemical signatures. Both mineral fractions are capable of reacting with the 1.0 N acetic acid applied for extracting the "carbonate fraction" in this study. Comparison of results between the 4-hour 1.0 N acetic acid step, and samples subjected to an additional 2 h exposure to 1.0 N acetic acid, shows that the first acetic acid step can be clearly distinguished as being a "carbonate fraction" while the additional exposure to acetic acid is contaminated with the "detrital fraction".

The Al/(Ca+Mg) in the 1.0 N acetic acid (extra 2 hours) extracted fractions are all greater than those in the 1.0 N acetic acid (first 4 hours) extracted fractions (**Figure A2**A). BSI and $^{87}Sr/^{86}Sr$ are also greater in the sample exposed for an additional 2 hours, and Y/Ho is lower. These trends are best explained by the preferential dissolution of detrital minerals such as clays in the sample exposed to acetic acid for an additional 2 hours, which does not occur in the prior 4 hour

extraction step. It is possible that the solutions are still acidic at the end of the first acetic acid exposure, thereby allowing for enhanced dissolution of non-carbonate phases. Fresh exposure of detrital materials due to removal of carbonates in the 1.0 N acetic acid 4h leach also could render them available for dissolution in the additional 2 h step. The end result is that Al, which is associated with detrital content, is preferentially released during the additional 2h acetic acid step.

Release of more radiogenic Sr with the additional 2h in 1.0 N acetic acid step further supports the observation that detrital mineral dissolution occurred during the sequential extractions, however did not significantly influence dissolved chemical species present in the carbonate fraction (first acetic acid step). A previous study (Phan et al., 2018b) showed that $^{87}Sr/^{86}Sr$ in the detrital minerals of the Marcellus Shale ranged from 0.711 to 0.723. Such $^{87}Sr/^{86}Sr$ range is much greater than the range of $^{87}Sr/^{86}Sr$ observed in the primary carbonate fraction of the Marcellus Shale samples analyzed in this study (0.708 – 0.713; **Fig. 8**B). These results allow for $^{87}Sr/^{86}Sr$ to be applied in differentiating the REY signal from carbonate minerals and detrital materials in shales.

To further ensure the reliability of using 1.0 N acetic acid (4 hours) in selectively extracting carbonate materials in shales, a second independent leaching procedure using 0.2 N nitric acid for 15 minutes (Tostevin et al., 2016) was applied on select samples. The limited volume of 0.2 N nitric acid was used to ensure incomplete dissolution of carbonate materials (Tostevin et al., 2016). We found that acetic acid leaches more Al from limestones than nitric acid but little difference exists between both procedures when applied to shales (**Fig. A2**; supporting materials). This is unexpected because dissolution of carbonate minerals in limestones buffers solution pH more than in shales, thus minimizing the risk of dissolution of non-carbonate materials (Tostevin et al., 2016). On the other hand, there is no observable difference in Y/Ho and $^{87}Sr/^{86}Sr$ between two leachate solutions of either 1.0 N acetic acid or 0.2 N nitric acid (**Fig. A2**; supporting materials) for both shales and limestones. However, the BSI in 0.2 N nitric acid leachates are slightly higher than those in the acetic acid leachates.

Overall, the reasonable consistency in REY patterns and $^{87}Sr/^{86}Sr$ in the carbonate leachates extracted by either procedure A or B suggests that the REY and $^{87}Sr/^{86}Sr$ of the primary carbonate fraction (Procedure A) represent the signatures of the target carbonate phase without

significant contamination from detrital materials. The variations in $^{87}Sr/^{86}Sr$ and REY signatures of carbonate cements in studied shales are much greater than any deviation induced by the dissolution of non-carbonate minerals, suggesting that partial leaching using 1.0 N acetic acid for 4 hours can be reliably done to evaluate carbonate diagenesis in shales.

4.2 Depositional environment of Marcellus Shale in the northeastern West Virginia – comparison to prior studies in other locations

The discussion in this section focuses on the depositional and diagenetic influences on the Marcellus MIP-3H core, which will be the focus of more detailed analysis in subsequent discussion sections. Previous studies on core materials from other regions of the Appalachian Basin showed that the Marcellus Shale was deposited under anoxic to euxinic (anoxic and sulfidic) conditions (Chen and Sharma, 2016; Lash and Blood, 2014; Phan et al., 2018b; Sageman et al., 2003; Ver Straeten et al., 2011; Werne et al., 2002) with intermitted episodes of dysoxic to perhaps oxic conditions, even in the organic-rich Union Springs member (Blood and Lash, 2015; Chen and Sharma, 2016). The following discussion outlines how results for the MIP-3H core compare to these prior studies.

We found a greater abundance of clastic sediment in the uppermost section compared to lower sections of the MIP-3H core, as demonstrated through the correlation between TiO_2 and Al_2O_3 (**Fig. 4**). The stepwise upward increase in clastic flux observed in the Marcellus Shale succession in the MIP-3H core is consistent with clastic flux observed in the Whipkey State #1 (WS) core (Chen and Sharma 2016). Even though the MIP-3H core in northeastern West Virginia is closer to the orogenic belt to the east than the WS core in Greene County, PA, USA (Chen and Sharma, 2016, 2017; Lash and Blood, 2014; Phan et al., 2018b), geochemical data demonstrated that the detrital input in MIP-3H core is very similar to the WS core. If wind-worked detritus/eolian input contributed to the clastic sediments, mineral sorting would be expected, thus, leading to variable Ti/Al in the sediment (Caplan and Bustin, 1998). However, a good correlation between Ti and Al (r^2=0.93; not shown) for all samples in MIP-3H core suggests that the fluxes of Ti containing minerals and clays are strongly linked together, likely from the same source. These detrital materials are predominantly from Grenville orogenic belt to the east of the depositional basin (Phan et al., 2018b).

The organic-rich portion of MIP-3H includes the Union Springs member and the basal section of the Lower Oatka Creek member (>2285 m; **Fig. 4**). Within this stratigraphic depth, large downward enrichment in U and Mo, and Si/Al was observed in comparison to the overlying organic poor portion. This observation is suggestive of reducing environment of bottom water established by enhanced biological production during deposition of this portion. High productivity in the surface water is also supported by correlations between TOC vs. Si/Al (r^2=0.36; not shown) and Fe/Al (r^2=0.74; not shown) in this section of MIP-3H. Assuming that the redox conditions during deposition correlate with the enrichment of U, Mo, and the accumulation of organic matter (i.e., TOC content), the base of the Union Springs member (~2299m) was under a more reducing environment during the early depositional stages of the Marcellus Shale.

Shales from MIP-3H core exhibit a strong enrichment of Mo relative to U at all EFs, indicating the operation of particulate shuttle (Tribovillard et al. 2012; Phan et al., 2018b) during the deposition of the Marcellus Shale. Particle scavenging of Mo operates when there is preferential adsorption of Mo onto metal-oxyhydroxides (e.g., Mn oxyhydroxide) and organic matter at the upper water column, and then adsorbed Mo was carried downward and accumulated as thiomolybdates under sulfidic and anoxic bottom water (Kendall et al., 2017). This mechanism exhibits little effect on aqueous U, thus enhancing the transfer of aqueous Mo to the sediment. Particularly, Mo-EF in the Union Springs member (Mo-EF=63 – 415) are much greater than the overlying Oatka Creek members. This is consistent with the trend observed in the Marcellus Shale in the southcentral and northeastern Appalachian Basin (Phan et al., 2018b). The large accumulation of U in this organic-rich portion occurred due to the reduction of U from seawater under anoxic conditions. Phan et al. (2018b) proposed that the reduction process was microbially mediated because of the large difference in U isotope composition between the shales and seawater. Further evidence of anoxic to euxinic bottom water conditions at the base of the Union Springs member is indicated by elevated Fe/Al (**Fig. 4**B). High Fe/Al in this portion likely coincides with the presence of abundant small size pyrite framboids in this section of WS core (Chen and Sharma, 2016; Lash and Blood, 2014).

In contrast to conditions during deposition of the organic-rich shale, the surface water productivity was plausibly lower during deposition of overlying organic-poor section as

indicated by its lower TOC content (**Fig. 3**B). Similarly, the enrichment of U and Mo is not as extensive in the organic poor portion, but still greater than 3 for U-EF and 88 for Mo-EF of most samples comprising the Upper Oatka Creek member (<2285 m). In this section, U concentration also correlates well with Mo (r^2=0.72), as well as the EFs (r^2=0.71; not shown). High U-EF and preferential enrichment of Mo relative to U, as observed in the Union Springs member, suggest that the reducing bottom water could have been intermittently rich in sulfide (Kendall et al., 2017). With one calcareous shale sample at depth 2271.9 m, U and Mo are solely derived from clastic sediment (U-EF=Mo-EF=1) which is also supported by high Th/U (Th/U=3). These geochemical data suggest that this section in the Upper Oatka Creek member was possibly deposited under oxidizing bottom water conditions. Under such conditions, authigenic accumulation of trace metals such as U and Mo is negligible because they occur predominantly as soluble complexes with either carbonate or stable molybdate ion (Langmuir, 1997).

In summary, the studied MIP-3H core in northeastern West Virginia reported in this study is closer to the orogenic highlands to the east than the WS core but received similar clastic flux. Geochemical data of MIP-3H core confirm that the organic-rich portion (base of the Lower Oatka Creek and Union Springs members) was deposited under more reducing bottom water conditions than the overlying organic poor portion. Elevated levels and fluctuation of U-EF and Mo-EF within the stratigraphic depth of the core indicate that bottom water redox conditions varied during the depositional period. This change could be due to higher clastic flux in the organic poor portion due to rising sea levels, or diminished productivity, or both.

4.3 Application of REY to characterize diagenetic processes

Results from both whole-rock and sequential extraction analyses show that detrital materials such as siliciclastic minerals, coupled with contributions from authigenic phases, are the main source of REY in both black shales and limestones analyzed in this study. Detailed analysis of REY in the authigenic phases (e.g., sequentially-extracted samples) helps to further explain diagenetic processes associated with the MIP-3H core.

4.3.1 Whole-rock REY

As discussed in 4.2, clastic flux increased upward in the MIP-3H core which explains the coinciding increasing trend of ΣREY in the Marcellus Shale in this core (**Fig. 5**B). When normalizing to Al, a detrital proxy, most shale samples fall on a vertical line in the depth profile

plot of ΣREY/Al (**Fig. 5**C). These observations suggest that the detrital materials in shales dominate the REY content with ΣREY/Al (ppm/ppm) = 0.0025±0.0006 (2SD; n=28) for most samples.

Some shale samples exhibit greater ΣREY/Al values, and all four analyzed calcareous shales have ΣREY/Al ranging from 0.0051 to 0.0085, which is five times greater than detrital dominated REY samples (ΣREY/Al = 0.0025±0.0006). This observation is further supported by the fact that the shale (PAAS) normalized patterns of these calcareous shales is higher than all black shales and displays a strong enrichment of HREE relative to LREE (**Fig. 7**B). The bulk P contents in these calcareous shales are similar to the black shales in this study (**Fig. 6**C) suggesting that phosphate minerals are not likely the primary cause of authigenic enrichment of REY in our studied samples. Moreover, the REY patterns of these calcareous shales are more similar to the seawater REY signature (Tepe and Bau, 2016) than the common MREE enrichment patterns of phosphate nodules (Zhang et al., 2016).

Neither organic matter (e.g., TOC) nor carbonate content exhibits any correlation with ΣREY. On the other hand, a moderate correlation between Al_2O_3 and ΣREY (r^2=0.52) indicates a primary detrital origin of REY in studied limestones and shales, with a likely contribution from authigenic phases.

4.3.2 REY in sequentially-extracted fractions

The REY in the water soluble, exchangeable, and primary carbonate fraction leachates are used to evaluate which authigenic components cause the enrichment in REY, particularly in the calcareous shales and one P-rich sample of the Marcellus Shale. Like previous work (Phan et al., 2018b), REY in the water-soluble and exchangeable fractions of the Marcellus Shale from MIP-3H core are negligible, <0.2% and <0.3%, respectively. The REY in water-soluble fractions are below the detection limits, and therefore not discussed here. The REY detected in the exchangeable fraction mimic a typical seawater REY pattern (e.g., Tepe and Bau, 2016), displaying negative Ce anomalies and HREE depletion (**Fig. 7**C). This reflects an influence of later fluid flow processes involving evaporated paleo-seawater due to the similarity with the seawater REY pattern. There are two possible explanations for the depletion of HREE in the exchangeable fractions of the Marcellus Shale: delayed desorption kinetics during the sequential

extraction, or incomplete preservation of seawater REY due to sorption phenomena associated with HREE.

Based on the model of lanthanides desorption from clays (Moldoveanu and Papangelakis, 2012) and the hydration energy of lanthanides (Habenschuss and Spedding, 1979a, b, 1980), LREE would be desorbed from the surface of clays faster (more preferentially) than HREE because the ionic hydration increases from La to Lu due to the contraction in ionic radii (Spedding et al., 1977). Moldoveanu and Papangelakis (2012) showed that desorption of REY from clays occurs quickly, less than 5 minutes to reach equilibrium stage. For comparison, our leaching procedure for cation exchange fraction was conducted for 4 hours in 1.0 N ammonium acetate at pH 8. This leaching time is much longer than the time needed to allow the desorption to complete. Thus, incomplete desorption (leaching process), particularly for HREE due to their higher hydration energies, is unlikely to be influencing the REY measured in the exchangeable fraction leachate.

The exchangeable REY data indicate that the REY signature in the diagenetic fluid was not fully preserved during adsorption. It is likely that the adsorption of HREE from the diagenetic fluid onto surfaces of organic matter and clays was limited due to higher hydration energies of HREE compared to LREE. Thus, the exchangeable fraction's seawater-like REY patterns with HREE depletion can be explained by the theoretical mechanism of REY adsorption on clays (Moldoveanu and Papangelakis, 2012) and by the diagenetic fluid likely consisting of evaporated seawater.

The carbonate cements of all black shales in the MIP-3H core consistently exhibit the enrichment of MREE (**Fig. 7**D). In contrast, REY patterns of the carbonates in calcareous shales and limestones exhibit HREE enrichment, LREE depletion, negative Ce anomalies, and slightly chondritic Y/Ho (31-37), which are like modern seawater REY signatures (**Fig. 7**D). No phosphate was detected by ion chromatography in the carbonate extracts of these calcareous shales (**Table S1**), thereby ruling out the contribution of phosphate minerals to the REY content in the carbonate fraction extracts. A previous study showed that the enrichment of MREE in both the remnant organic matter and carbonate cement fractions of the Marcellus Shale likely reflects the interactions between diagenetic pore fluid (a precursor of carbonate cement) and the organic matter in the shale during diagenesis (Phan et al., 2018b).

Carbonate concretions are found in four calcareous shale lenses (**Fig. 2**A) in both Oatka Creek and Union Springs members. In these lenses, the carbonates contain seawater-like REY patterns to some extent which are distinct from the MREE enrichment patterns of carbonate cements in black shales in surrounding depths. These thin lenses of calcium carbonate concretions at ~2272, 2276, 2288, and 2298 m (**Fig. 2**A) could possibly be derived from high alkalinity pore fluid that preserved the signature of seawater. It has been proposed that the carbonate concretions (e.g., calcareous shales in this study) in the Marcellus Shale could have been derived from the anaerobic oxidation of methane in the sulfate-reducing zone, producing high alkalinity and sulfide-rich porewater (Lash and Blood, 2014; Chen and Sharma 2016). This mechanism is also supported by $^{87}Sr/^{86}Sr$ data, showing that $^{87}Sr/^{86}Sr$ values in the carbonate of calcareous shales (0.7081 – 0.7087) are very close to unaltered Middle Devonian carbonates (0.7076 – 0.7079; Diener et al., 1996).

Authigenic carbonate minerals tend to dominate the bulk rock REY inventory of calcareous shales. Unlike carbonate cements, the carbonate concretions extracted from the calcareous shales are more concentrated in REY, which contributes 37 – 54% of REY of the whole-rock. Similarly, as shown in **Fig. A1**B, ΣREY*1000/(Ca+Mg) of calcareous shales are greater than 1 whereas ΣREY*1000/(Ca+Mg) of carbonate cements are less than 1. Therefore, the REY in carbonate cements possibly reflects complex alteration processes after their formation. This indicates a greater influence of diagenesis on black shale geochemistry.

Several hypotheses explaining the mechanisms of MREE enrichments in the black shale carbonate cements are considered. It is possible for the MREE enriched signature in carbonate cements to be derived from the organic matter during thermal maturation in the Marcellus Shale, as previously proposed in Phan et al. (2018b). The results from this study (Phan et al., 2018b) corroborates with Freslon et al. (2014) that documented MREE enrichment in modern sedimentary organic matter. It is unlikely that MREE enrichments of REY in the Marcellus Shale was caused by adsorption onto Fe- and Mn- oxyhydroxide surfaces (Gutjahr et al., 2007; Haley et al., 2004) as it was deposited under anoxic to euxinic conditions (Blood and Lash, 2015; Chen and Sharma, 2016; Lash and Blood, 2014; Phan et al., 2018b; Sageman et al., 2003; Werne et al., 2002), not conducive to Fe- and Mn-oxyhydroxide formation. The exact mechanism(s) explaining the similarity in the MREE enriched patterns between carbonate cement and remnant

organic matter in the Marcellus Shale remains unclear. However, we postulate that the diagenetic process were post depositional: the carbonate cement was either formed much later (when sediment column was more compacted) than the carbonate concretions in calcareous shales, or significantly altered by diagenesis in shales during burial, or a combination of both processes.

4.4 Post-depositional alteration of carbonate cement in black shales

The carbonate in limestones likely formed by direct precipitation from seawater based on the $^{87}Sr/^{86}Sr$ signatures, and the REY in the methane-derived authigenic carbonates in the calcareous shales are mainly derived of diagenetic porewater originating from paleo-seawater, with minimal influence of later diagenesis. The $^{87}Sr/^{86}Sr$ values in the primary carbonate fraction of Tully and Cherry Valley limestones and calcareous shales are close to $^{87}Sr/^{86}Sr$ (0.7076 – 0.7079) of unaltered carbonate minerals precipitated from the Middle Devonian seawater (Diener et al., 1996). Likewise, the REY patterns of these carbonate (HREE enrichment relative to LREE, BSI<2, **Fig. 7**D) to some extent resemble modern seawater REY signature (Tepe and Bau, 2016). With an exception, the Y/Ho in carbonates in limestones (31-37) and calcareous shales (27-30) which are generally lower than hydrogenous carbonates (Y/Ho > 36; Tostevin et al., 2016).

The $\delta^{13}C$ measured in carbonate concretions and the Cherry Valley limestone appears to contradict the above conclusion, as the values are much lower than unaltered Middle Devonian carbonates (Saltzman, 2005) (**Fig. 5**D). Overall, $\delta^{13}C$ values do not follow any trend with depth or $^{87}Sr/^{86}Sr$ (**Fig. 5**D). We propose that the carbon isotope signature is affected by upward methane flux in the sediment column and across buried strata, which can fluctuate and hence does not faithfully reflect the chemistry of the local porewater at a specific stratigraphic depth. Because of the potential complications involved with applying $\delta^{13}C$ to understand diagenetic influence on the system, we are considering $^{87}Sr/^{86}Sr$ signature in carbonate as more conservative indicator of chemical evolution of carbonates in the system.

In contrast to observations for the carbonate concretions, carbonate cements in black shales appear to be significantly influenced by diagenesis. Results from both this study and a prior study (Phan et al., 2018c) show that Sr/Ca by weight (0.001 – 0.005) in carbonate cements of the Marcellus Shale do not vary stratigraphically and geographically across the Appalachian Basin. However, $^{87}Sr/^{86}Sr$ in carbonate cements of black shales (0.7085 – 0.713) exhibit a good and negative correlation with sample depth (r^2=0.66; not shown), and more radiogenic Sr was found

in the shallower depth. This trend indicates the release of more radiogenic Sr into the pore fluid without inducing a significant change in Sr/Ca (**Fig. 8**C), consistent with Stewart et al., (2015). If the pore fluid was mixed well in the sediment column, a uniform $^{87}Sr/^{86}Sr$ value in the carbonate cements would be expected. Thus, the observed variation in $^{87}Sr/^{86}Sr$ (**Fig. 8**B) suggests that the porewater was not mixed and was affected locally by the surrounding minerals.

Expulsion of radiogenic isotope ^{87}Sr during the transformation of clays from smectite to illite (Chaudhuri and Clauer, 1993; Osborn et al., 2012) can explain high $^{87}Sr/^{86}Sr$ in the carbonate cement (**Fig. 8**B). This mechanism was also proposed by Stewart et al. (2015) for explaining the enrichment of radiogenic Sr in carbonate cements in the Marcellus Shale in the northeastern Appalachian Basin (NE site; **Fig. 1**). Our results also show that carbonate cements in the Oatka Creek members are more radiogenic (higher in $^{87}Sr/^{86}Sr$) and display more bell-shaped REY patterns (higher in BSI) compared to the Union Springs members (**Fig. 5**E; **Table 2**). A good correlation (r^2=0.70; not shown) between $^{87}Sr/^{86}Sr$ and BSI in the carbonate cements suggests that high $^{87}Sr/^{86}Sr$ and high BSI (i.e., generation of MREE enrichment) in carbonate cements are controlled either by the same process, or different processes occurring under similar burial conditions.

Many studies (Clauer et al., 2018; Pagel et al., 1997; Williams and Hervig, 2005) have shown that illite-smectite transformation occurs at the same diagenetic temperature and pressure conditions that generate hydrocarbons (oil and gas) from kerogen. Because carbonate cement and the remnant organic matter both displayed MREE enriched pattern in a prior study on Marcellus Shale (Phan et al., 2018b), it is reasonable to assume that REY in these two pools was derived from the same source. During the illite-smectite transition, the REY with MREE enrichment was possibly released from smectite into pore fluid which was then incorporated into the remnant organic matter during catagenesis, and later preserved in the resulting carbonate cement. This clay transition process also expelled more radiogenic Sr (Chaudhuri and Clauer, 1993; Osborn et al., 2012) into the pore fluid, explaining the greater $^{87}Sr/^{86}Sr$ values in carbonate cements compared to the carbonate concretions or adjacent limestone units in this study. A schematic model explaining the diagenetic alteration of carbonate minerals during diagenesis and catagenesis in the Appalachian Basin is shown in Figure 9.

5 Conclusions

This study investigated the sources, distribution, and diagenetic modification of sedimentary rocks in the Appalachian Basin. The results demonstrated that authigenic components in the samples provide more detailed information regarding depositional and diagenetic processes occurring in the sedimentary rocks.

Geochemical signatures from carbonate versus detrital mineral fractions in this study were distinguishable by the sequential extraction procedures. Fairly consistent REY patterns and $^{87}Sr/^{86}Sr$ were observed in the carbonates of shales extracted by either 1.0 N acetic acid for 4 hours or 0.2 N nitric acid for 15 minutes. The reproducible results obtained by two leaching methods indicate that REY and $^{87}Sr/^{86}Sr$ in the 1.0 N leachates represent the genuine signatures of the target carbonates in analyzed rocks. However, additional leaching for 2h with acetic acid induced dissolution of clays. Dissolution of detrital minerals led to the preferential release of MREE, decrease in Y/Ho, and release of more radiogenic Sr. Thus, partial leaching using 1.0 N acetic acid for 4 hours is recommended for extracting REY and $^{87}Sr/^{86}Sr$ from the carbonate minerals in shales and limestones, to avoid contamination from detrital phases during longer leaching periods.

The detailed analysis for the MIP-3H core is relatable to other studies on depositional and diagenetic history of the Marcellus Shale. Progradation of the clastic sediment (Sageman et al. 2003)) from the Grenville orogenic belt (Phan et al., 2018b) during the Middle Devonian age is also observed in the Marcellus Shale in our studied core (MIP-3H) in the northeast of West Virginia. Even though this core is in proximity to the highlands to the east, the amount of the clastic flux in this core is similar to the WS core which is more distal to the detrital sediment source. The organic-rich portion (base of the Lower Oatka Creek and Union Springs members) was deposited under more reducing bottom water conditions than the overlying organic poor portion. High and alternating enrichments of U and Mo within the stratigraphic depth of the core demonstrate that bottom water redox conditions varied during the depositional period, possibly alternating between persistently anoxic in the Union Springs member to intermitted episodes of dysoxic/oxic conditions in the Upper Oatka Creek member.

The REY in Marcellus Shale is primarily derived from detrital materials in which ΣREY/Al (ppm/ppm) = 0.0025±0.0006 (2SD; n=28). This study suggests that this value can be used to

infer the contribution of authigenic REY in shales. Unlike carbonate cements, methanogenic derived carbonate minerals in calcareous shales (carbonate concretions) are more concentrated in REY which contributes 37 – 54% of REY of bulk rocks and dominates the bulk rock REY inventory of calcareous shales.

This study showed a proof-of-concept of a new approach that the bell-shaped indices (BSI) of the carbonate minerals can be used to evaluate the degree of diagenetic influence in shales. The greater value of BSI infers a greater influence of post-depositional processes on the carbonate minerals in shales. The results of this study also suggest that the $^{87}Sr/^{86}Sr$ in carbonates is more conservative in preserving the chemistry of precursor fluid than $\delta^{13}C$, particularly for investigating the diagenetic influence/origin of carbonate minerals. Even though the carbonates in calcareous shales shared some features ($^{87}Sr/^{86}Sr$, REY) similar to seawater, these carbonates do not entirely inherit paleo-seawater chemistry and could have been influenced by diagenesis to some extent (however not as much as in carbonate cements). Therefore, caution should be exercised in applying REY patterns in carbonate minerals for reconstruction of paleo redox conditions or paleo-seawater chemistry.

As a record of the smectite to illite transition, which relates to thermal maturation of kerogen within the shale, the authigenic phases provide an important view into historic geologic processes contributing to current unconventional oil and gas reservoirs. A positive correlation between the bell-shaped indices and $^{87}Sr/^{86}Sr$ in the carbonate minerals in the Marcellus Shale reflects the concurrent source of REY and radiogenic Sr (^{87}Sr) in the pore fluid during diagenetic smectite-illite transformation. This process likely released more MREE into pore fluid, thus explaining the enrichment of the MREE in carbonate cements. Under similar temperature and pressure conditions of catagenesis, the REY enriched in MREE in porewater could be likely incorporated and preserved in the remnant organic matter in black shales.

Acknowledgements

This study was supported by the U.S. Department of Energy, Office of Fossil Energy, as the National Energy Technology Laboratory's ongoing research. Samples for this research were provided by the Marcellus Shale Energy and Environment Laboratory (MSEEL) funded by Department of Energy's National Energy Technology Laboratory (DOE-NETL) grant DE# FE0024297. We thank Drs. B. Stewart and R. Capo for providing clean lab space for sample preparation, Dr. D. Bain for technical support with ICP-MS analysis, Dr. Z. Karpynand for providing two Marcellus Shale samples from Tioga County, PA, USA, Dr. D. Crandall for

providing samples from MIP-SW core, C. Hite for assistance with radiogenic Sr isotope analysis. The authors thank reviewers for constructive feedback and Dr. Jérôme Gaillardet for handling the manuscript. This research was supported in part by appointment to the National Energy Technology Laboratory Research Participation Program, sponsored by the U.S. Department of Energy and administered by the Oak Ridge Institute for Science and Education (TTP).

Disclaimers

Any opinions, findings, conclusions, or recommendations expressed herein are those of the authors and do not necessarily reflect the views of the sponsors. Reference in this paper to any specific commercial product, process, or service is to facilitate understanding and does not imply endorsement by the United States Department of Energy.

References

Agrawal V and Sharma S, 2018. Molecular Characterization of Kerogen from Mature Marcellus Shale and its Implications for Determining Hydrocarbon Potential and Thermal Maturity. Fuel 228: 429–437.

Agrawal, V. and Sharma, S. 2018. Pitfalls in modeling physico-chemical properties of Shale using kerogen type. Nature Scientific Reports (in review).

Algeo, T.J., Tribovillard, N., 2009. Environmental analysis of paleoceanographic systems based on molybdenum–uranium covariation. Chem. Geol. 268, 211-225.

Auer, G., Reuter, M., Hauzenberger, C.A., Piller, W.E., 2017. The impact of transport processes on rare earth element patterns in marine authigenic and biogenic phosphates. Geochim. Cosmochim. Acta 203, 140-156.

Blakey, R. (2013). North America Paeogeography <http://cpgeosystems.com/nam.html> (accessed 06/25/2015).

Blood, D.R., Lash, G.G., 2015. Dynamic redox conditions in the Marcellus Shale as recorded by pyrite framboid size distributions. Geological Society of America Special Papers 515, 153-168.

Caplan, M.L., Bustin, R.M., 1998. Sedimentology and sequence stratigraphy of Devonian-Carboniferous strata, southern Alberta. Bulletin of Canadian Petroleum Geology 46, 487-514.

Chaudhuri, S., Clauer, N., 1993. Strontium isotopic compositions and potassium and rubidium contents of formation waters in sedimentary basins: Clues to the origin of the solutes. Geochim. Cosmochim. Acta 57, 429-437.

Chen, R., Sharma, S., 2016. Role of alternating redox conditions in the formation of organic-rich interval in the Middle Devonian Marcellus Shale, Appalachian Basin, USA. Palaeogeogr., Palaeoclimatol., Palaeoecol. 446, 85-97.

Chen, R., Sharma, S., 2017. Linking the Acadian Orogeny with organic-rich black shale deposition: Evidence from the Marcellus Shale. Mar. Pet. Geol. 79, 149-158.

Chung, F.H., 1974. Quantitative interpretation of X-ray diffraction patterns of mixtures. I. Matrix-flushing method for quantitative multicomponent analysis. J. Appl. Crystallogr. 7, 519-525.

Clauer, N., Williams, L.B., Lemarchand, D., Florian, P., Honty, M., 2018. Illitization decrypted by B and Li isotope geochemistry of nanometer-sized illite crystals from bentonite beds, East Slovak Basin. Chem. Geol. 477, 177-194.

Diener, A., Ebneth, S., Veizer, J., Buhl, D., 1996. Strontium isotope stratigraphy of the Middle Devonian: Brachiopods and conodonts. Geochim. Cosmochim. Acta 60, 639-652.

Dulski, P., 1994. Interferences of oxide, hydroxide and chloride analyte species in the determination of rare earth elements in geological samples by inductively coupled plasma-mass spectrometry. Fresenius J. Anal. Chem. 350, 194-203.

Freslon, N., Bayon, G., Toucanne, S., Bermell, S., Bollinger, C., Chéron, S., Etoubleau, J., Germain, Y., Khripounoff, A., Ponzevera, E., Rouget, M.-L., 2014. Rare earth elements and neodymium isotopes in sedimentary organic matter. Geochim. Cosmochim. Acta 140, 177-198.

Gutjahr, M., Frank, M., Stirling, C.H., Klemm, V., van de Flierdt, T., Halliday, A.N., 2007. Reliable extraction of a deepwater trace metal isotope signal from Fe–Mn oxyhydroxide coatings of marine sediments. Chem. Geol. 242, 351-370.

Habenschuss, A., Spedding, F.H., 1979a. The coordination (hydration) of rare earth ions in aqueous chloride solutions from x- ray diffraction. II. $LaCl_3$, $PrCl_3$, and $NdCl_3$. The Journal of Chemical Physics 70, 3758-3763.

Habenschuss, A., Spedding, F.H., 1979b. The coordination (hydration) of rare earth ions in aqueous chloride solutions from x ray diffraction. I.$TbCl_3$,$DyCl_3$, $ErCl_3$,$TmCl_3$,and $LuCl_3$. The Journal of Chemical Physics 70, 2797-2806.

Habenschuss, A., Spedding, F.H., 1980. The coordination (hydration) of rare earth ions in aqueous chloride solutions from x- ray diffraction. III. $SmCl_3$, $EuCl_3$, and series behavior. The Journal of Chemical Physics 73, 442-450.

Haley, B.A., Klinkhammer, G.P., McManus, J., 2004. Rare earth elements in pore waters of marine sediments. Geochim. Cosmochim. Acta 68, 1265-1279.

Kendall, B., Dahl, T.W., Anbar, A.D., 2017. The stable isotope geochemistry of molybdenum. Reviews in Mineralogy and Geochemistry 82, 683-732.

Kolesar Kohl, C.A., Capo, R.C., Stewart, B.W., Wall, A.J., Schroeder, K.T., Hammack, R.W., Guthrie, G.D., 2014. Strontium Isotopes Test Long-Term Zonal Isolation of Injected and Marcellus Formation Water after Hydraulic Fracturing. Environ. Sci. Technol. 48, 9867-9873.

Langmuir, D., 1997. Aqueous environmental geochemistry. Prentice Hall, Upper Saddle River New Jersey.

Lash, G.G., Blood, D.R., 2014. Organic matter accumulation, redox, and diagenetic history of the Marcellus Formation, southwestern Pennsylvania, Appalachian basin. Mar. Pet. Geol. 57, 244-263.

Macquaker, J.H., Adams, A., 2003. Maximizing information from fine-grained sedimentary rocks: an inclusive nomenclature for mudstones. Journal of Sedimentary Research 73, 735-744.

Milliken, K.L., Rudnicki, M., Awwiller, D.N., Zhang, T., 2013. Organic matter-hosted pore system, Marcellus Formation (Devonian), Pennsylvania. AAPG Bulletin 97, 177-200.

Moldoveanu, G.A., Papangelakis, V.G., 2012. Recovery of rare earth elements adsorbed on clay minerals: I. Desorption mechanism. Hydrometallurgy 117–118, 71-78.

Neymark, L.A., Premo, W.R., Mel'nikov, N.N., Emsbo, P., 2014. Precise determination of $\delta^{88}Sr$ in rocks, minerals, and waters by double-spike TIMS: a powerful tool in the study of geological, hydrological and biological processes. J. Anal. At. Spectrom. 29, 65-75.

Niu, D., Renock, D., Whitehouse, M., Leone, J., Rowe, H., Landis, J., Hamren, K., Symcox, C.W., Sharma, M., 2016. A relict sulfate–methane transition zone in the mid-Devonian Marcellus Shale. Geochim. Cosmochim. Acta 182, 73-87.

Osborn, S.G., McIntosh, J.C., Hanor, J.S., Biddulph, D., 2012. Iodine-129, $^{87}Sr/^{86}Sr$, and trace elemental geochemistry of northern Appalachian Basin brines: Evidence for basinal-scale fluid migration and clay mineral diagenesis. Am. J. Sci. 312, 263-287.

Pagel, M., Braun, J.-J., Disnar, J.R., Martinez, L., Renac, C., Vasseur, G., 1997. Thermal history constraints from studies of organic matter, clay minerals, fluid inclusions, and apatite fission tracks at the Ardeche paleo-margin (BA1 drill hole, GPF Program), France. Journal of Sedimentary Research 67.

Paronish, T., 2018. Meso- and Macro-scale Facies and Chemostratigraphic Analysis of Middle Devonian Marcellus Shale in Northern West Virginia, USA. West Virginia University, Morgantown, West Virginia, USA (382 pp.).

Phan, T.T., Bain, D.J., Hakala, A.J., 2018a. Influence of colloids on metal concentrations and radiogenic strontium isotopes in groundwater and oil and gas-produced waters. Appl. Geochem. 85, 85-96.

Phan, T.T., Capo, R.C., Stewart, B.W., Graney, J.R., Johnson, J.D., Sharma, S., Toro, J., 2015. Trace metal distribution and mobility in drill cuttings and produced waters from Marcellus Shale gas extraction: Uranium, arsenic, barium. Appl. Geochem. 60, 89-103.

Phan, T.T., Capo, R.C., Stewart, B.W., Macpherson, G., Rowan, E.L., Hammack, R.W., 2016. Factors controlling Li concentration and isotopic composition in formation waters and host rocks of Marcellus Shale, Appalachian Basin. Chem. Geol. 420, 162-179.

Phan, T.T., Gardiner, J.B., Capo, R.C., Stewart, B.W., 2018b. Geochemical and multi-isotopic ($^{87}Sr/^{86}Sr$, $^{143}Nd/^{144}Nd$, $^{238}U/^{235}U$) perspectives of sediment sources, depositional conditions, and diagenesis of the Marcellus Shale, Appalachian Basin, USA. Geochim. Cosmochim. Acta 222, 187-211.

Phan, T.T., Paukert Vankeuren, A.N., Hakala, J.A., 2018c. Roles of water–rock interactions in the geochemical evolution of Marcellus Shale produced waters. International Journal of Coal Geology 191, 95-111.

Pourmand, A., Dauphas, N., Ireland, T.J., 2012. A novel extraction chromatography and MC-ICP-MS technique for rapid analysis of REE, Sc and Y: Revising CI-chondrite and Post-Archean Australian Shale (PAAS) abundances. Chem. Geol. 291, 38-54.

Sageman, B.B., Murphy, A.E., Werne, J.P., Ver Straeten, C.A., Hollander, D.J., Lyons, T.W., 2003. A tale of shales: the relative roles of production, decomposition, and dilution in the accumulation of organic-rich strata, Middle–Upper Devonian, Appalachian basin. Chem. Geol. 195, 229-273.

Saltzman, M.R., 2005. Phosphorus, nitrogen, and the redox evolution of the Paleozoic oceans. Geology 33, 573-576.

Shields, G., Stille, P., 2001. Diagenetic constraints on the use of cerium anomalies as palaeoseawater redox proxies: an isotopic and REE study of Cambrian phosphorites. Chem. Geol. 175, 29-48.

Spedding, F.H., Rard, J.A., Habenschuss, A., 1977. Standard state entropies of the aqueous rare earth ions. The Journal of Physical Chemistry 81, 1069-1074.

Stewart, B.W., Chapman, E.C., Capo, R.C., Johnson, J.D., Graney, J.R., Kirby, C.S., Schroeder, K.T., 2015. Origin of brines, salts and carbonate from shales of the Marcellus Formation: Evidence from geochemical and Sr isotope study of sequentially extracted fluids. Appl. Geochem. 60, 77-88.

Tepe, N., Bau, M., 2016. Behavior of rare earth elements and yttrium during simulation of arctic estuarine mixing between glacial-fed river waters and seawater and the impact of inorganic (nano-) particles. Chem. Geol. 438, 134-145.

Tissot, B., Welte, D., 2012. Petroleum formation and occurrence: a new approach to oil and gas exploration. Springer Science & Business Media.

Tostevin, R., Shields, G.A., Tarbuck, G.M., He, T., Clarkson, M.O., Wood, R.A., 2016. Effective use of cerium anomalies as a redox proxy in carbonate-dominated marine settings. Chem. Geol. 438, 146-162.

Tribovillard, N., Algeo, T.J., Baudin, F., Riboulleau, A., 2012. Analysis of marine environmental conditions based onmolybdenum–uranium covariation – Applications to Mesozoic paleoceanography. Chem. Geol. 324–325, 46-58.

Tribovillard, N., Algeo, T.J., Lyons, T., Riboulleau, A., 2006. Trace metals as paleoredox and paleoproductivity proxies: An update. Chem. Geol. 232, 12-32.

Ver Straeten, C.A., Brett, C.E., Sageman, B.B., 2011. Mudrock sequence stratigraphy: A multi-proxy (sedimentological, paleobiological and geochemical) approach, Devonian Appalachian Basin. Palaeogeogr., Palaeoclimatol., Palaeoecol. 304, 54-73.

Wall, A.J., Capo, R.C., Stewart, B.W., Phan, T.T., Jain, J.C., Hakala, J.A., Guthrie, G.D., 2013. High throughput method for Sr extraction from variable matrix waters and $^{87}Sr/^{86}Sr$ isotope analysis by MC-ICP-MS. J. Anal. At. Spectrom. 28, 1338-1344.

Wei, L., Mastalerz, M., Schimmelmann, A., Chen, Y., 2014. Influence of Soxhlet-extractable bitumen and oil on porosity in thermally maturing organic-rich shales. International Journal of Coal Geology 132, 38-50

Werne, J.P., Sageman, B.B., Lyons, T.W., Hollander, D.J., 2002. An integrated assessment of a "type euxinic" deposit: Evidence for multiple controls on black shale deposition in the middle Devonian Oatka Creek formation. Am. J. Sci. 302, 110-143.

Whitacre, J.V. (2014). Carnegie Museum of Natural History Pennsylvania Unconventional Natural Gas Wells Geodatabase (v.2014-Q4) [Computer File]. Carnegie Museum of Natural History, Pittsburgh, PA <http://www.carnegiemnh.org/science/default.aspx?id=18716> (accessed 13.07.14).

Williams, L.B., Hervig, R.L., 2005. Lithium and boron isotopes in illite-smectite: The importance of crystal size. Geochim. Cosmochim. Acta 69, 5705-5716.

Williams, L.B., Środoń, J., Huff, W.D., Clauer, N., Hervig, R.L., 2013. Light element distributions (N, B, Li) in Baltic Basin bentonites record organic sources. Geochim. Cosmochim. Acta 120, 582-599.

Willis, S.S., Johannesson, K.H., 2011. Controls on the geochemistry of rare earth elements in sediments and groundwaters of the Aquia aquifer, Maryland, USA. Chem. Geol. 285, 32-49.

Yang, J., Torres, M., McManus, J., Algeo, T.J., Hakala, J.A., Verba, C., 2017. Controls on rare earth element distributions in ancient organic-rich sedimentary sequences: Role of post-depositional diagenesis of phosphorus phases. Chem. Geol. 466, 533-544.

Zhang, K., Zhu, X.-K., Yan, B., 2015. A refined dissolution method for rare earth element studies of bulk carbonate rocks. Chem. Geol. 412, 82-91.

Zhang, L., Algeo, T.J., Cao, L., Zhao, L., Chen, Z.-Q., Li, Z., 2016. Diagenetic uptake of rare earth elements by conodont apatite. Palaeogeogr., Palaeoclimatol., Palaeoecol. 458, 176-197.

Zhu, B., Jiang, S.-Y., Yang, J.-H., Pi, D., Ling, H.-F., Chen, Y.-Q., 2014. Rare earth element and SrNd isotope geochemistry of phosphate nodules from the lower Cambrian Niutitang Formation, NW Hunan Province, South China. Palaeogeogr., Palaeoclimatol., Palaeoecol. 398, 132-143.

Figure Captions

Figure 1. The Middle Devonian paleogeography map modified after Blakey (2013) (a) and the present-day map modified after Whitacre (2014) (b) show the geographic location of the Marcellus Shale Energy and Environment Laboratory (MSEEL) site (filled circle) in Monongalia County, WV, USA. At MSEEL site, two adjacent cores (MIP-3H and MIP-SW) within 800 m from each other were recovered for this study. High resolution samples were collected along the entire length of MIP-3H core (Upper and Lower Oatka Creek members, Cherry Valley limestone, and Union Springs member) and samples of underlying and overlying formations (Mahantango Shale, Tully limestone, Burket Shale) were collected from the adjacent MIP-SW core. In addition, two Marcellus Shale samples were collected from a core in TG site (open circle) in Tioga County, PA, USA. The locations of SC (filled star) and NE site (open star), previously reported in Phan et al., (2018b), are shown for reference. Gamma ray logs of MIP-3H and MIP-SW drill cores in MSEEL site are from Paronish (2018).

Figure 2. Three parallel sequential extraction procedures used in this study.

Figure 3. Depth profiles of carbonate contents (wt. %), TOC contents (wt. %), and TiO_2 (wt. %), Al_2O_3 (wt. %), and SiO_2 (wt. %) of whole rock samples as detrital proxies for MIP-3H core in Monongalia County, WV, USA. The carbonate contents as CaCO3 and MgCO3 are calculated based on the concentrations of Ca and Mg in the primary carbonate fraction (1.0 N acetic acid for 4 hours). Whole rock Mo (ppm) and U (ppm) concentrations correlate well with TOC (wt. %). Gamma-ray log is from Paronish (2018). Simplified stratigraphy is based on the mineralogical compositions of the samples reported in this study.

Figure 4. Variation in Si/Al (A), Fe/Al (B), Th/U (C) of bulk rocks and the enrichment factors of U (D) and Mo (E) in whole rock samples of MIP-3H core in Monongalia County, WV, USA.

Figure 5. Variation in P (A), ΣREY (B), ΣREY/Al (C) of bulk rocks, $\delta^{13}C$ of the primary carbonates (D), and $^{87}Sr/^{86}Sr$ (E) of the primary carbonate fraction (Procedure A: 1.0 N acetic acid, 4 hours; **Fig. 2**) with depth. Ranges of $\delta^{13}C$, ca. 0 – 1‰ (Saltzman, 2005) and $^{87}Sr/^{86}Sr$, 0.7076 – 0.7079 (Diener et al., 1996) values of unaltered Middle Devonian carbonates (within the thickness of the bars, D and E) are shown for comparison.

Figure 6. Cross-plots showing the relationships between carbonate contents (A), Al_2O_3 (B), P (C), and TOC (D) with ΣREY in bulk rocks. The carbonate contents (wt. %) as $CaCO_3$ and $MgCO_3$ are calculated based on the concentrations of Ca and Mg in the primary carbonate fraction (1.0 N acetic acid for 4 hours). The linear trend line (r^2=0.52) in (C) is plotted for all analyzed samples except the four calcareous shales.

Figure 7. Chondrite-normalized (A) and post Archean Australian Shale (PAAS) normalized REY patterns of whole rock (B), exchangeable fraction (adsorbed REY; C) and primary carbonate fraction (D) (Procedure A in Figure 2) of all samples reported in this study. The REY data of chondrite and PAAS (Table S1, supporting material) are from Pourmand et al. (2012). The REY data of North Atlantic coastal seawater are from Tepe and Bau (2016). Dotted line and pointing down arrows depict the depletion of HREE in the exchangeable fractions of all analyzed samples relative to seawater. The data plotted in these figures are reported in the supporting materials.

Figure 8. Cross-plots showing the relationships between bell-shaped index (BSI) vs. the carbonate content (A) and $^{87}Sr/^{86}Sr$ vs. Sr/Rb in the primary carbonate fraction (B). The BSI of modern North Atlantic coastal seawater (Tepe and Bau, 2016) and Onondaga limestones (diamond symbol; Phan et al. (2018b)) are shown for comparison. The $^{87}Sr/^{86}Sr$ of unaltered carbonate end-member = 0.7076 – 0.7079 (Diener et al., 1996) and its Sr/Rb is presumed. The dashed line reflects the diagenetic evolution of an unaltered carbonate end-member toward an extremely modified carbonate end-member (high $^{87}Sr/^{86}Sr$ and low Sr/Rb). The solid arrow represents the addition of ^{87}Sr, possibly expelled from clays during smectite-illite transformation.

Figure 9. A schematic diagram explaining the diagenetic alteration of carbonates in shales and limestones of the Appalachian Basin based on the results of this study and a previous study (Phan et al., 2018b). Primary carbonate minerals (Procedure A, Figure 2) of black shales, calcareous shales, and limestones are referred to as carbonate cement, carbonate concretion, and limestone carbonate, respectively.

Table Captions

Table 1. Semi-quantitative mineralogical composition (weight %) of selected samples reported in this study

Table 2. Total organic carbon, carbonate, major, minor, and rare earth element concentrations in whole rocks

Sample ID	Well name (API number)	Coordinate	Location	Formation	Quartz %	Muscovite/lillite %	Chlorite %	Calcite %	Dolomite %	Pyrite %	Barite %	Albite %	Marcasite %	K-feldspar %	Gypsum %
MIP3H-11	MIP-3H (4706101707)	39°36'06.5"N 79°58'34.0"W	Monongalia Co., WV, USA	Marcellus Shale	38	33	10	15	3.0	1.0	n/d	n/d	n/d	n/d	n/d
MIP3H-23	MIP-3H (4706101707)	39°36'06.5"N 79°58'34.0"W	Monongalia Co., WV, USA	Marcellus Shale	31	30	9.5	18	2.9	3.8	n/d	n/d	n/d	n/d	n/d
MIP3H-31	MIP-3H (4706101707)	39°36'06.5"N 79°58'34.0"W	Monongalia Co., WV, USA	Marcellus Shale	30	48	8.5	0.9	n/d	3.8	2.8	n/d	n/d	n/d	n/d
MIP3H-36	MIP-3H (4706101707)	39°36'06.5"N 79°58'34.0"W	Monongalia Co., WV, USA	Marcellus Shale	37	48	7.8	1.0	n/d	2.9	n/d	n/d	n/d	n/d	n/d
MIP3H-65	MIP-3H (4706101707)	39°36'06.5"N 79°58'34.0"W	Monongalia Co., WV, USA	Marcellus Shale	44	31	n/d	10	1.9	5.6	n/d	n/d	n/d	n/d	n/d
MIP3H-89	MIP-3H (4706101707)	39°36'06.5"N 79°58'34.0"W	Monongalia Co., WV, USA	Marcellus Shale	35	47	n/d	7.6	0.9	3.8	n/d	n/d	n/d	n/d	n/d
MIP3H-99	MIP-3H (4706101707)	39°36'06.5"N 79°58'34.0"W	Monongalia Co., WV, USA	Marcellus Shale	30	38	n/d	17	0.9	4.5	n/d	n/d	n/d	n/d	n/d
SW-44	MIP-SW (4706101705)	39°36'32.0"N 79°58'47.7"W	Monongalia Co., WV, USA	Burket Shale	32	48	6.7	1.0	n/d	2.9	n/d	4.8	1.0	n/d	n/d
SW-36	MIP-SW (4706101705)	39°36'32.0"N 79°58'47.7"W	Monongalia Co., WV, USA	Shale	29	50	5.8	n/d	n/d	2.9	n/d	7.7	n/d	n/d	1.9
SW-21	MIP-SW (4706101705)	39°36'32.0"N 79°58'47.7"W	Monongalia Co., WV, USA	Mahantango Shale	31	48	8.9	n/d	n/d	2.0	n/d	7.9	n/d	n/d	1.0
SW-17	MIP-SW (4706101705)	39°36'32.0"N 79°58'47.7"W	Monongalia Co., WV, USA	Mahantango Shale	33	48	7.9	n/d	n/d	2.0	n/d	6.9	n/d	n/d	1.0
SW-5	MIP-SW (4706101705)	39°36'32.0"N 79°58'47.7"W	Monongalia Co., WV, USA	Marcellus Shale	40	44	10.0	2.0	3.0	1.0	n/d	n/d	n/d	n/d	n/d
MS-Slab1	n/a	n/a	Tioga Co., PA, USA	Marcellus Shale	29	44	6.0	6.9	3.0	3.0	n/d	7.9	n/d	n/d	n/d
MS-Slab2	n/a	n/a	Tioga Co., PA, USA	Marcellus Shale	33	46	3.8	1.0	1.9	2.9	n/d	7.7	n/d	n/d	n/d

n/d= not detected; n/a = not available; note: the percentage of minerals are normalized to (100%-%TOC)

Table 1

Sample ID	Well name	Location	Formation	Rock Type	Depth	Carbonate[a]	TOC	P	Na	Mg	Al	Si	K	Ca	Ti	Fe	Mo	Th	U	∑REY[b]	∑REY/Al	Fe/Al	Th/U	U-EF	Mo-EF	∑REY in primary carbonate[b]	% of ∑REY in primary carbonate
					m	%	%	ppm	ppm	ppm	ppm	ppm	ppm	ppm	ppm	ppm	ppm	ppm	ppm	ppm						ppm	
MIP3H-4	MIP-3H	Monongalia Co., WV, USA	Marcellus Shale	Shale	2269.9	0.43	3.26	310	4600	780	9650	29700	3450	5350	450	4420	59	11	10	225.4	0.0023	0.46	1.20	3	33	5	2
MIP3H-7	MIP-3H	Monongalia Co., WV, USA	Marcellus Shale	Shale	2270.8	0.86	2.64	444	4510	710	8660	29900	3050	7530	400	5230	53	10	7	223.4	0.0026	0.60	1.33	3	33	11	5
MIP3H-11	MIP-3H	Monongalia Co., WV, USA	Marcellus Shale	Calcareous shale	2271.9	26.5	0.45	319	2220	810	6550	20500	1940	8110	350	5320	2	8	3	331.5	0.0051	0.81	2.95	1	1	129	39
MIP3H-13	MIP-3H	Monongalia Co., WV, USA	Marcellus Shale	Shale	2272.5	0.50	3.61	358	4640	720	9510	28300	3280	5200	430	4840	94	11	13	226.7	0.0024	0.51	0.83	4	53	9	4
MIP3H-16	MIP-3H	Monongalia Co., WV, USA	Marcellus Shale	Shale	2273.5	0.28	4.46	367	4420	790	10200	26500	3610	5100	450	4620	116	6	11	17	266.5	0.0026	0.45	0.68	5	60	7	3
MIP3H-20	MIP-3H	Monongalia Co., WV, USA	Marcellus Shale	Shale	2274.6	1.24	3.84	378	4730	780	10300	27000	3650	7810	420	4250	92	11	16	257.6	0.0025	0.41	0.69	5	47	15	6
MIP3H-23	MIP-3H	Monongalia Co., WV, USA	Marcellus Shale	Calcareous shale	2275.6	25.3	4.80	359	3050	740	6770	18500	2350	7100	290	4110	89	7	23	402.2	0.0059	0.61	0.31	11	70	219	54
MIP3H-28	MIP-3H	Monongalia Co., WV, USA	Marcellus Shale	Shale	2277.0	0.37	5.10	358	4540	710	9670	25400	3450	5900	410	4350	144	10	26	232.9	0.0024	0.45	0.38	9	79	9	4
MIP3H-31	MIP-3H	Monongalia Co., WV, USA	Marcellus Shale	Shale	2277.9	0.98	5.31	1500	4470	730	9780	25200	3520	7400	420	4770	137	10	31	332.4	0.0034	0.49	0.33	10	75	39	12
MIP3H-33	MIP-3H	Monongalia Co., WV, USA	Marcellus Shale	Shale	2278.5	2.19	3.83	420	4520	780	12000	30700	3710	5800	530	7120	124	12	21	245.5	0.0020	0.59	0.57	6	55	23	9
MIP3H-36	MIP-3H	Monongalia Co., WV, USA	Marcellus Shale	Shale	2279.4	0.46	3.03	325	5170	710	10500	29100	3710	6800	480	3780	63	11	10	195.1	0.0019	0.36	1.07	3	32	6	3
MIP3H-42	MIP-3H	Monongalia Co., WV, USA	Marcellus Shale	Shale	2281.1	0.50	3.38	321	5210	760	9980	29800	3550	5610	450	4170	100	10	16	233.4	0.0023	0.42	0.63	5	53	6	3
MIP3H-45	MIP-3H	Monongalia Co., WV, USA	Marcellus Shale	Shale	2282.1	1.29	2.90	284	4790	850	9830	28500	3470	5900	450	4310	96	10	11	225.5	0.0023	0.44	0.90	3	52	7	3
MIP3H-47	MIP-3H	Monongalia Co., WV, USA	Marcellus Shale	Shale	2282.8	0.99	3.87	321	5130	800	9920	28700	3560	8300	480	4310	118	10	15	248.0	0.0025	0.44	0.70	5	63	10	4
MIP3H-50	MIP-3H	Monongalia Co., WV, USA	Marcellus Shale	Shale	2283.6	1.74	4.31	312	4990	790	9710	28000	3430	8400	420	3800	88	9	14	232.9	0.0024	0.39	0.66	5	65	13	6
MIP3H-53	MIP-3H	Monongalia Co.,	Marcellus Shale	Shale	2284.6	6.28	4.35	443	4300	670	8060	24800	2850	4002	600	7130	133	8	25	246.1	0.0031	0.88	0.32	10	88	25	10

		WV, USA	Shale												0													
		Monong	Marcel												39													
MIP3H	MIP-	alia Co.,	lus					423	61	674	271	239	70	31	431	15								12			
-56	3H	WV, USA	Shale	Shale	2285.5	6.01	6.28	345	0	40	40	100	70	0	90	50	1	7	25	200.4	0.0030	0.64	0.28	12	0	20	10
		Monong	Marcel										22															
MIP3H	MIP-	alia Co.,	lus					360	60	626	307	227	53	29	362	15								12			
-59	3H	WV, USA	Shale	Shale	2286.3	3.95	7.16	447	0	10	20	700	40	0	70	90	0	7	24	223.6	0.0036	0.58	0.27	13	8	24	11
		Monong	Marcel																									
MIP3H	MIP-	alia Co.,	lus					436	58	729	307	263	80	36	571	14								10			
-62	3H	WV, USA	Shale	Shale	2287.1	1.35	5.43	447	0	70	30	000	40	10	80	70	3	8	23	236.0	0.0032	0.78	0.35	10	5	11	5
		Monong	Marcel	Calcar										78														
MIP3H	MIP-	alia Co.,	lus	eous					304	58	505	253	176	13	24	501	17								18			
-65	3H	WV, USA	Shale	shale	2288.1	15.6	7.40	892	0	20	80	000	60	0	40	80	0	5	45	379.2	0.0075	0.99	0.12	29	0	139	37
		Monong	Marcel										23															
MIP3H	MIP-	alia Co.,	lus					373	63	684	300	255	70	33	391	18								14			
-70	3H	WV, USA	Shale	Shale	2289.6	3.53	7.90	530	0	00	50	700	90	0	80	00	6	8	33	263.5	0.0039	0.57	0.23	15	6	34	13
		Monong	Marcel										34															
MIP3H	MIP-	alia Co.,	lus					441	69	768	282	293	76	39	397	18								12			
-72	3H	WV, USA	Shale	Shale	2290.1	5.18	6.22	611	0	60	30	600	10	0	70	10	1	9	27	224.3	0.0029	0.52	0.32	11	6	16	7
		Monong	Marcel										55															
MIP3H	MIP-	alia Co.,	lus					425	86	662	229	244	42	36	540	11												
-75	3H	WV, USA	Shale	Shale	2291.0	9.27	5.74	396	0	00	40	200	00	0	10	90	9	7	14	185.1	0.0028	0.82	0.53	7	96	26	14
		Monong	Marcel										22															
MIP3H	MIP-	alia Co.,	lus					578	69	845	278	326	02	47	351	10												
-78	3H	WV, USA	Shale	Shale	2291.9	3.66	6.88	547	0	20	80	500	50	0	40	60	0	10	17	239.6	0.0028	0.42	0.60	7	63	17	7
		Monong												33														
MIP3H	MIP-	alia Co.,	Cherry	Limes						38	682	274	248	44	51	190												
-80	3H	WV, USA	Valley	tone	2292.5	72.0	2.00	618	740	40	0	00	0	20	0	10	5	1	2	85.3	0.0125	2.79	0.71	9	39	57	67
		Monong	Marcel										45															
MIP3H	MIP-	alia Co.,	lus					451	60	743	278	289	65	40	356													
-84	3H	WV, USA	Shale	Shale	2293.7	7.24	5.46	383	0	90	30	700	10	0	60	70	87	8	15	225.1	0.0030	0.48	0.56	6	63	38	17
		Monong	Marcel										21															
MIP3H	MIP-	alia Co.,	lus					449	52	721	281	274	20	35	484													
-86	3H	WV, USA	Shale	Shale	2294.3	2.15	4.46	403	0	50	50	000	80	0	80	30	94	8	16	168.9	0.0023	0.67	0.50	7	70	14	8
		Monong	Marcel										54															
MIP3H	MIP-	alia Co.,	lus					463	57	706	278	281	46	36	339	12												
-89	3H	WV, USA	Shale	Shale	2295.2	9.50	5.51	361	0	40	00	300	20	0	40	00	7	8	16	205.8	0.0029	0.48	0.49	7	96	46	22
		Monong	Marcel										17															
MIP3H	MIP-	alia Co.,	lus					489	56	757	308	290	84	38	337	12												
-91	3H	WV, USA	Shale	Shale	2295.8	1.95	6.03	600	0	90	60	000	40	0	10	50	7	8	27	196.4	0.0026	0.45	0.31	11	90	12	6
		Monong	Marcel										13															
MIP3H	MIP-	alia Co.,	lus					502	67	768	272	302	88	36	473	25								17			
-94	3H	WV, USA	Shale	Shale	2296.8	1.68	8.59	380	0	90	80	300	80	0	00	80	5	8	59	221.3	0.0029	0.62	0.14	25	7	10	5
		Monong	Marcel	Calcar										12														
MIP3H	MIP-	alia Co.,	lus	eous					342	42	374	218	147	11	19	402	14								20			
-99	3H	WV, USA	Shale	shale	2298.2	24.7	9.71	442	0	30	20	300	70	70	00	30	2	5	46	318.9	0.0085	1.08	0.10	39	3	135	42
		Monong	Marcel										51															
MIP3H	MIP-	alia Co.,	lus					361	43	394	195	150	55	20	702									12			
-101	3H	WV, USA	Shale	Shale	2298.8	4.06	7.54	482	0	30	10	300	70	0	10	00	90	4	39	174.6	0.0044	1.78	0.11	31	3	20	12
		Monong	Marcel										33															
MIP3H	MIP-	alia Co.,	lus					333	81	520	261	211	33	24	576	34								35			
-102.2	3H	WV, USA	Shale	Shale	2299.0	4.74	12.0	412	0	70	10	200	40	0	20	40	3	6	75	211.1	0.0041	1.11	0.08	46	2	18	8
		Monong	Marcel										32															
MIP3H	MIP-	alia Co.,	lus	Limes				192		24	320	118	109	76	14	304								10	41		
-110	3H	WV, USA	Shale	tone	2301.6	62.1	9.40	0	460	60	0	500	0	10	0	0	25	0	10	186.4	0.0583	0.95	0.03	2	5	125	67
		Monong	Marcel										63															
MIP3H	MIP-	alia Co.,	lus					415	94	572	262	242	19	31	312	31								29			
-112	3H	WV, USA	Shale	Shale	2302.1	11.3	5.37	579	0	50	30	700	00	0	10	10	5	6	32	131.7	0.0023	0.55	0.19	18	4	19	14
		Monong																										
	MIP-	alia Co.,	Burket						575	88	954	281	329	71	46	495	10											
SW-44	SW	WV, USA	Shale	Shale	2178.4	0.54	4.49	552	0	90	60	800	80	70	20	30	8	10	16	243.2	0.0025	0.52	0.62	5	61	5	2

SW-37	MIP-SW	Monongalia Co., WV, USA	Burket Shale	Shale	2179.2	0.03	6.67	692	6040	7960	9170	2800	3100	6340	4390	4160	1604	910	2727	227.7	0.0025	0.45	0.35	9	96	3	1
SW-36	MIP-SW	Monongalia Co., WV, USA	Burket Shale	Shale	2179.3	0.06	4.67	686	7490	7720	9450	2650	3200	7311 0	4460	5420	6800	1010	1827	201.7	0.0021	0.57	0.54	6	38	3	1
SW-31	MIP-SW	Monongalia Co., WV, USA	Tully Limestone	Limestone	2180.2	69.4	<0.5	352	1320	5740	2390	8440	8750	3311 0	6000	1090	1013	1	3	1	134.6	0.0056	0.45	3.36	1	2	90	67
SW-27	MIP-SW	Monongalia Co., WV, USA	Tully Limestone	Limestone	2185.7	73.1	<0.5	380	1170	6150	7020	5320	5760	3512 0	6095	1110	2012	1	2	1	112.5	0.0072	0.71	1.55	3	4	72	64
SW-26	MIP-SW	Monongalia Co., WV, USA	Tully Limestone	Limestone	2188.8	46.9	0.79	474	2710	5610	9020	1560	1820	3725 000	6270	2460	2070	5	6	3	149.3	0.0028	0.47	1.77	2	5	61	41
SW-21	MIP-SW	Monongalia Co., WV, USA	Mahantango Shale	Shale	2207.1	0.30	1.14	561	5960	9870	1040	3060	3460	6250	4570	4910	2050	2	10	3	213.2	0.0020	0.47	3.31	1	1	4	2
SW-17	MIP-SW	Monongalia Co., WV, USA	Mahantango Shale	Shale	2222.3	0.08	1.07	412	5250	9300	1080	2840	3720	5850	5120	4520	2600	1	2	1	112.5	0.0000	0.42	2.68	1	1	3	1
SW-13	MIP-SW	Monongalia Co., WV, USA	Mahantango Shale	Shale	2236.0	1.43	0.63	462	4940	1201 0	1090	2990	3700	6010	5240	4720	1007	2	4	3	239.3	0.0022	0.43	3.45	1	3	5	2
SW-5	MIP-SW	Monongalia Co., WV, USA	Marcellus Shale	Shale	2295.1	4.91	<0.5	138 0	5310	1200	7850	3110	2810	3890	4460	4490	1003	3	10	3	252.7	0.0032	0.57	3.50	1	2	29	12
MS-Slab1	n/a	Tioga Co., PA, USA	Marcellus Shale	Shale	1672.8	12.6	0.82	422	5660	1200	8790	2390	2840	1676 0	4160	4230	1010	10	9	4	226.6	0.0026	0.48	2.43	1	6	28	12
MS-Slab2	n/a	Tioga Co., PA, USA	Marcellus Shale	Shale	1692.4	1.92	4.21	418	6780	8500	8530	2910	2820	3916 0	4150	4590	1408	8	9	22	256.8	0.0030	0.54	0.41	8	93	6	3

bdl = below detection limit; n/a = not available; ppm = mg/kg

USGS rock reference standards including Green River Shale (SGR-1b), Brush Creek Shale (SBC-1), Icelandic Basalt (BIR-1a), and USGS spring waters (T-221 and T227) were analyzed as quality control samples during the course of the analysis. Based on the measured values of these reference samples, the accuracy of elemental concentration data is estimated to be better than 10% for major and minor elements and all rare earth elements except Dy, Er (within 20%).

[a]Carbonate content is calculated based on the concentrations of Ca, as $CaCO_3$, and Mg, as $MgCO_3$, extracted in 1.0N CH_3COOH leachate (4 hours)

[b]Elemental data including REY in whole rock and leachates are reported in the supporting materials

Table 2

Highlights

- A sequential extraction method was applied to separate authigenic minerals
- Authigenic components provide more detailed insights onto depositional environments and diagenesis in sedimentary rocks
- Carbonate cement in black shales is significantly altered during illite-smectite transition and catagenesis
- Carbonate minerals in limestones is minimally altered during burial compared to carbonate concretions and carbonate cement
- Intermitted episodes of dysoxic/oxic environment occurred during the deposition of the Upper Oatka Creek member

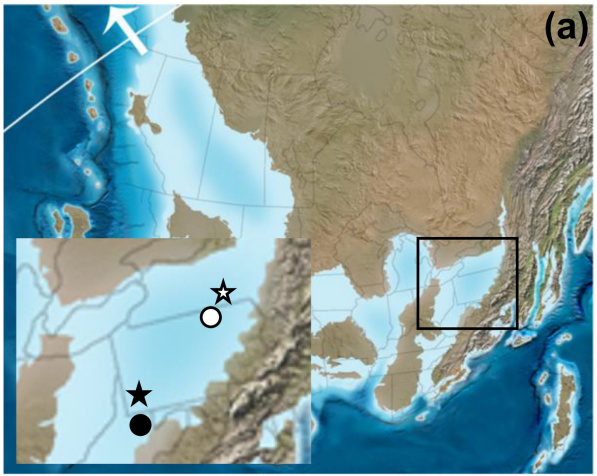

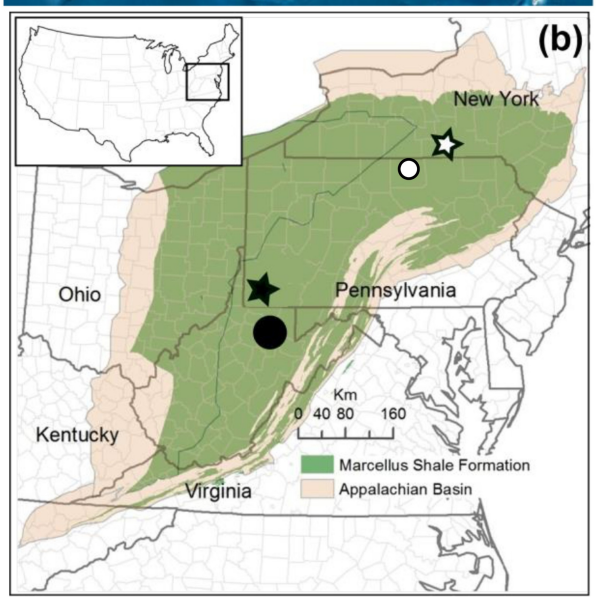

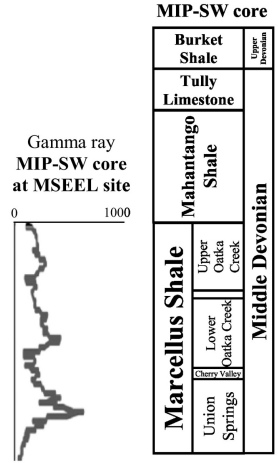

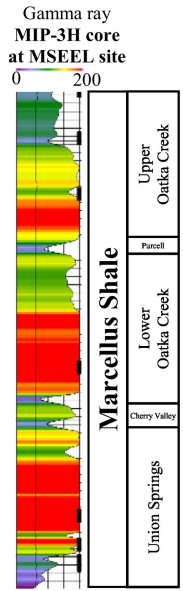

● : MSEEL site (this study)

○ : TG site (this study)

★ : SC site (Phan et al., 2018b)

☆ : NE site (Phan et al., 2018b)

Figure 1

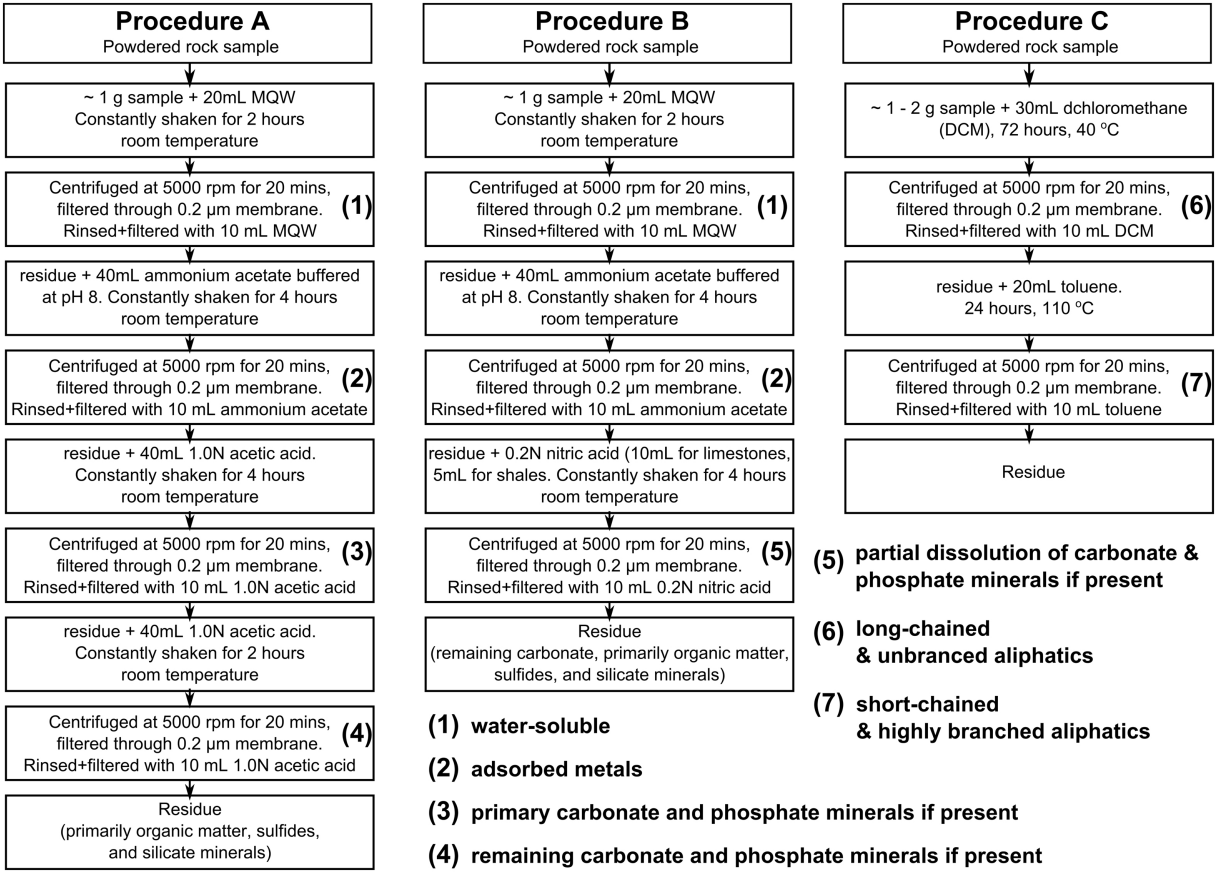
Procedure A
Powdered rock sample
~ 1 g sample + 20mL MQW
Constantly shaken for 2 hours
room temperature
Centrifuged at 5000 rpm for 20 mins,
filtered through 0.2 µm membrane.
Rinsed+filtered with 10 mL MQW
(1)
residue + 40mL ammonium acetate buffered
at pH 8. Constantly shaken for 4 hours
room temperature
Centrifuged at 5000 rpm for 20 mins,
filtered through 0.2 µm membrane.
Rinsed+filtered with 10 mL ammonium acetate
(2)
residue + 40mL 1.0N acetic acid.
Constantly shaken for 4 hours
room temperature
Centrifuged at 5000 rpm for 20 mins,
filtered through 0.2 µm membrane.
Rinsed+filtered with 10 mL 1.0N acetic acid
(3)
residue + 40mL 1.0N acetic acid.
Constantly shaken for 2 hours
room temperature
Centrifuged at 5000 rpm for 20 mins,
filtered through 0.2 µm membrane.
Rinsed+filtered with 10 mL 1.0N acetic acid
(4)
Residue
(primarily organic matter, sulfides,
and silicate minerals)
Procedure B
Powdered rock sample
~ 1 g sample + 20mL MQW
Constantly shaken for 2 hours
room temperature
Centrifuged at 5000 rpm for 20 mins,
filtered through 0.2 µm membrane.
Rinsed+filtered with 10 mL MQW
(1)
residue + 40mL ammonium acetate buffered
at pH 8. Constantly shaken for 4 hours
room temperature
Centrifuged at 5000 rpm for 20 mins,
filtered through 0.2 µm membrane.
Rinsed+filtered with 10 mL ammonium acetate
(2)
residue + 0.2N nitric acid (10mL for limestones,
5mL for shales. Constantly shaken for 4 hours
room temperature
Centrifuged at 5000 rpm for 20 mins,
filtered through 0.2 µm membrane.
Rinsed+filtered with 10 mL 0.2N nitric acid
(5)
Residue
(remaining carbonate, primarily organic matter,
sulfides, and silicate minerals)
Procedure C
Powdered rock sample
~ 1 - 2 g sample + 30mL dchloromethane
(DCM), 72 hours, 40 °C
Centrifuged at 5000 rpm for 20 mins,
filtered through 0.2 µm membrane.
Rinsed+filtered with 10 mL DCM
(6)
residue + 20mL toluene.
24 hours, 110 °C
Centrifuged at 5000 rpm for 20 mins,
filtered through 0.2 µm membrane.
Rinsed+filtered with 10 mL toluene
(7)
Residue
(1) water-soluble
(2) adsorbed metals
(3) primary carbonate and phosphate minerals if present
(4) remaining carbonate and phosphate minerals if present
(5) partial dissolution of carbonate & phosphate minerals if present
(6) long-chained & unbranced aliphatics
(7) short-chained & highly branched aliphatics

Figure 2

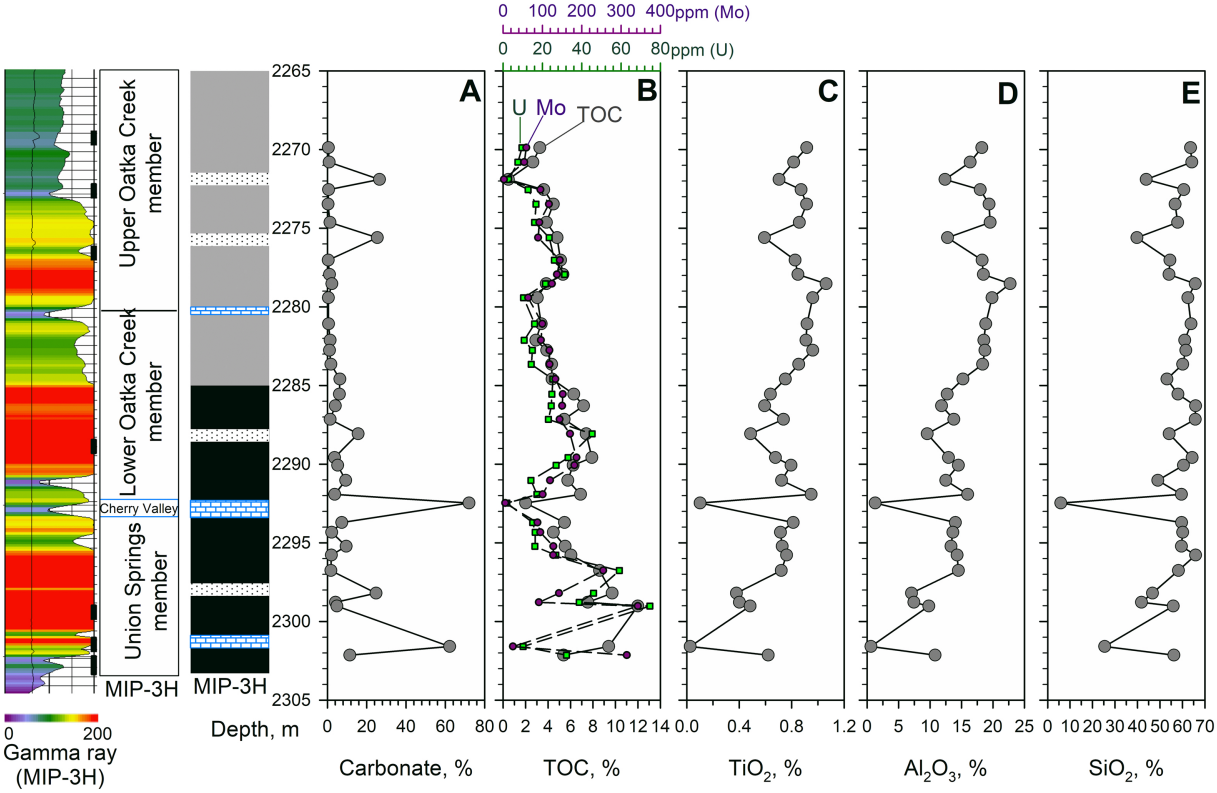
0 100 200 300 400ppm (Mo)
0 20 40 60 80ppm (U)
Upper Oatka Creek member
Lower Oatka Creek member
Cherry Valley
Union Springs member
MIP-3H
MIP-3H
0 200
Gamma ray (MIP-3H)
Depth, m
2265
2270
2275
2280
2285
2290
2295
2300
2305
A
B
C
D
E
U Mo TOC
0 20 40 60 80
Carbonate, %
0 2 4 6 8 10 12 14
TOC, %
0.0 0.4 0.8 1.2
TiO2, %
0 5 10 15 20 25
Al2O3, %
0 10 20 30 40 50 60 70
SiO2, %
Organic poor shale
Organic rich shale
Calcareous shale
Limestone

Figure 3

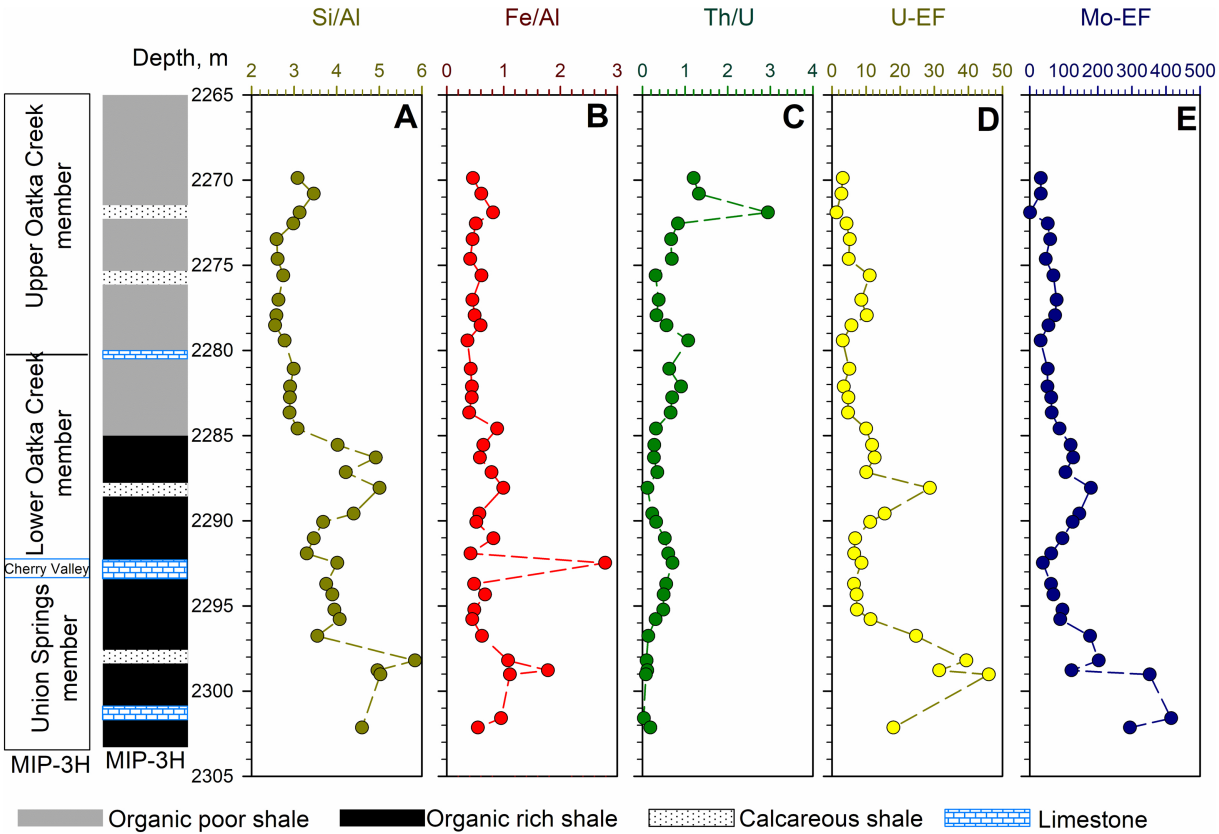
Si/Al
Fe/Al
Th/U
U-EF
Mo-EF
Depth, m
2 3 4 5 6
0 1 2 3
0 1 2 3 4
0 10 20 30 40 50
0 100 200 300 400 500
2265
2270
2275
2280
2285
2290
2295
2300
2305
A
B
C
D
E
Upper Oatka Creek member
Lower Oatka Creek member
Cherry Valley
Union Springs member
MIP-3H
MIP-3H
Organic poor shale
Organic rich shale
Calcareous shale
Limestone

Figure 4

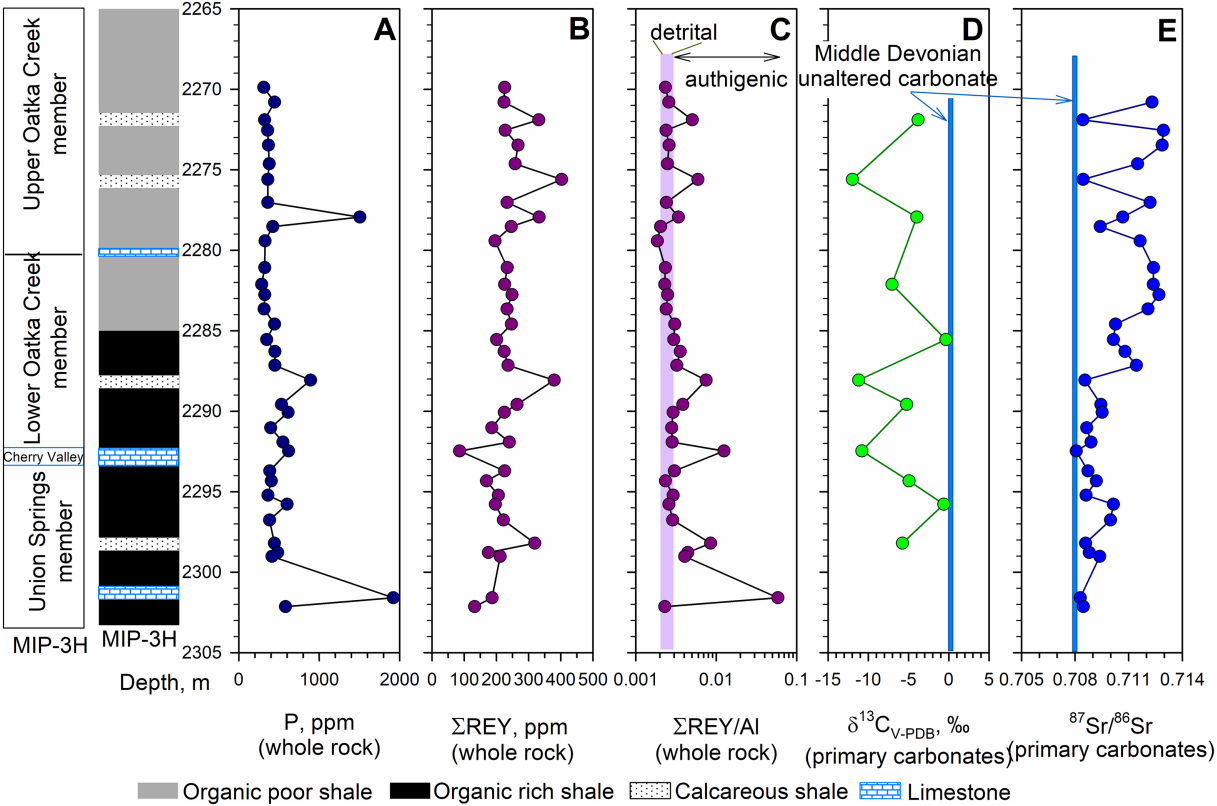
Upper Oatka Creek member
Lower Oatka Creek member
Cherry Valley
Union Springs member
MIP-3H
MIP-3H
Depth, m
2265
2270
2275
2280
2285
2290
2295
2300
2305
A
B
C
D
E
detrital
authigenic
Middle Devonian unaltered carbonate
0
1000
2000
0
100
200
300
400
500
0.001
0.01
0.1
-15
-10
-5
0
5
0.705
0.708
0.711
0.714
P, ppm (whole rock)
ΣREY, ppm (whole rock)
ΣREY/Al (whole rock)
δ13CV-PDB, ‰ (primary carbonates)
87Sr/86Sr (primary carbonates)
Organic poor shale
Organic rich shale
Calcareous shale
Limestone

Figure 5

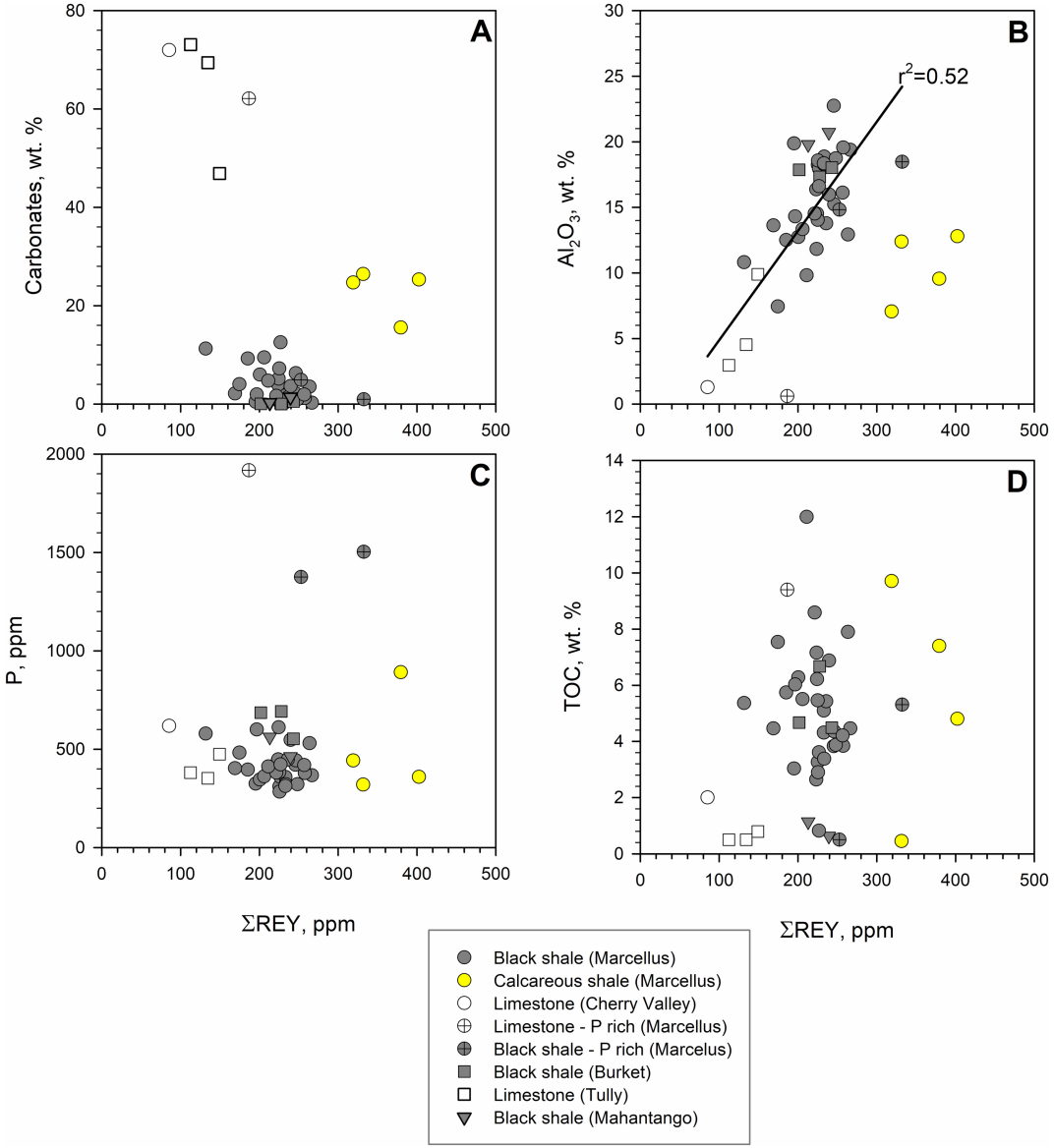
A
Carbonates, wt. %
B
Al_2O_3, wt. %
r^2=0.52
C
P, ppm
D
TOC, wt. %
ΣREY, ppm
ΣREY, ppm
Black shale (Marcellus)
Calcareous shale (Marcellus)
Limestone (Cherry Valley)
Limestone - P rich (Marcellus)
Black shale - P rich (Marcelus)
Black shale (Burket)
Limestone (Tully)
Black shale (Mahantango)

Figure 6

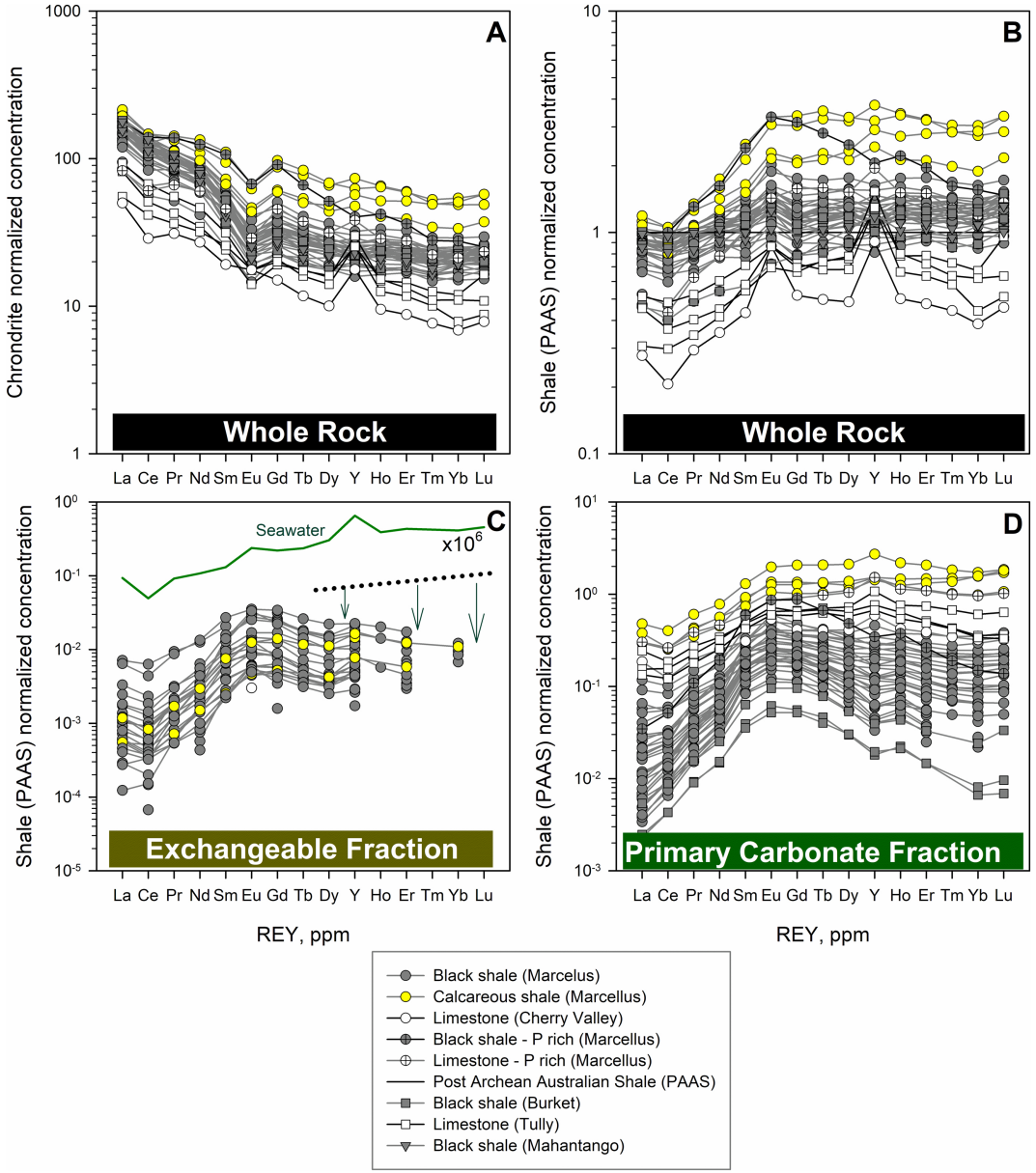
A
Chrondrite normalized concentration
1000
100
10
1
Whole Rock
La Ce Pr Nd Sm Eu Gd Tb Dy Y Ho Er Tm Yb Lu
B
Shale (PAAS) normalized concentration
10
1
0.1
Whole Rock
La Ce Pr Nd Sm Eu Gd Tb Dy Y Ho Er Tm Yb Lu
C
Seawater
x10^6
Shale (PAAS) normalized concentration
10^0
10^-1
10^-2
10^-3
10^-4
10^-5
Exchangeable Fraction
La Ce Pr Nd Sm Eu Gd Tb Dy Y Ho Er Tm Yb Lu
REY, ppm
D
Shale (PAAS) normalized concentration
10^1
10^0
10^-1
10^-2
10^-3
Primary Carbonate Fraction
La Ce Pr Nd Sm Eu Gd Tb Dy Y Ho Er Tm Yb Lu
REY, ppm
Black shale (Marcelus)
Calcareous shale (Marcellus)
Limestone (Cherry Valley)
Black shale - P rich (Marcellus)
Limestone - P rich (Marcellus)
Post Archean Australian Shale (PAAS)
Black shale (Burket)
Limestone (Tully)
Black shale (Mahantango)

Figure 7

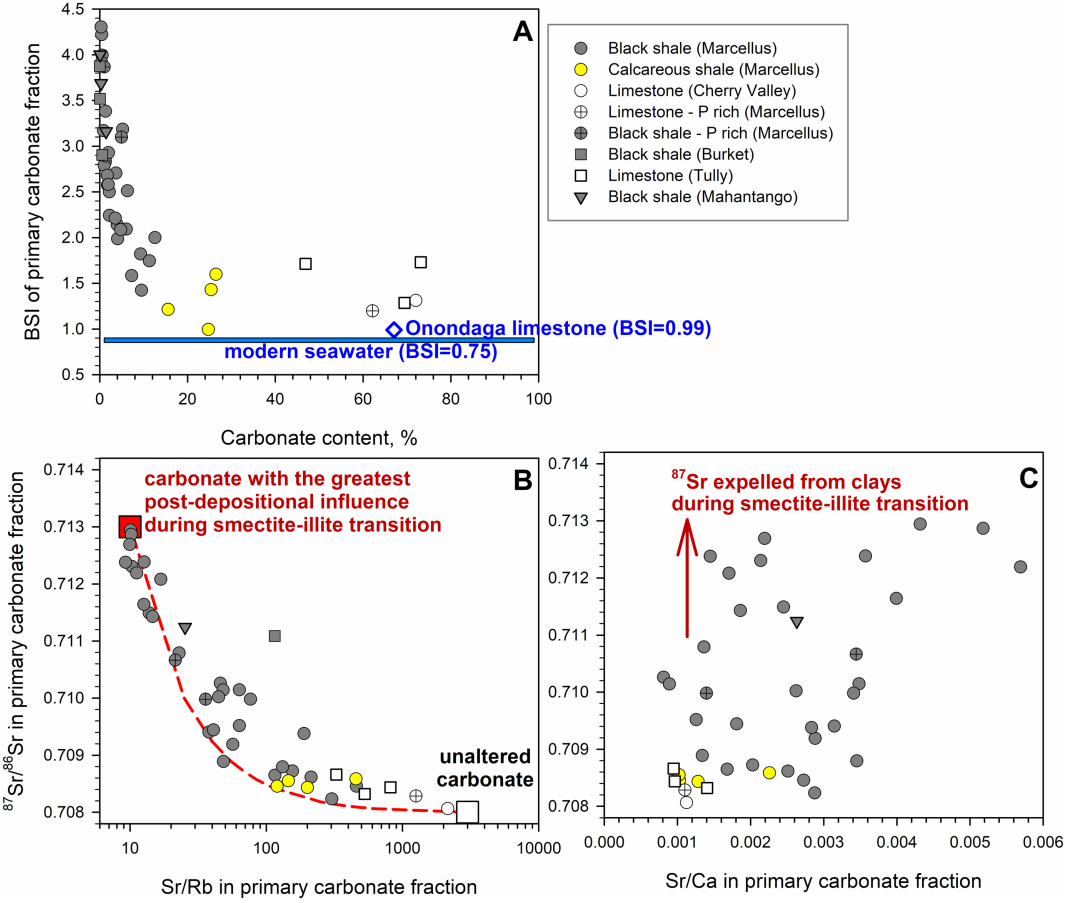
A
BSI of primary carbonate fraction
Carbonate content, %
Black shale (Marcellus)
Calcareous shale (Marcellus)
Limestone (Cherry Valley)
Limestone - P rich (Marcellus)
Black shale - P rich (Marcellus)
Black shale (Burket)
Limestone (Tully)
Black shale (Mahantango)
Onondaga limestone (BSI=0.99)
modern seawater (BSI=0.75)
B
carbonate with the greatest post-depositional influence during smectite-illite transition
unaltered carbonate
87Sr/86Sr in primary carbonate fraction
Sr/Rb in primary carbonate fraction
C
87Sr expelled from clays during smectite-illite transition
Sr/Ca in primary carbonate fraction

Figure 8

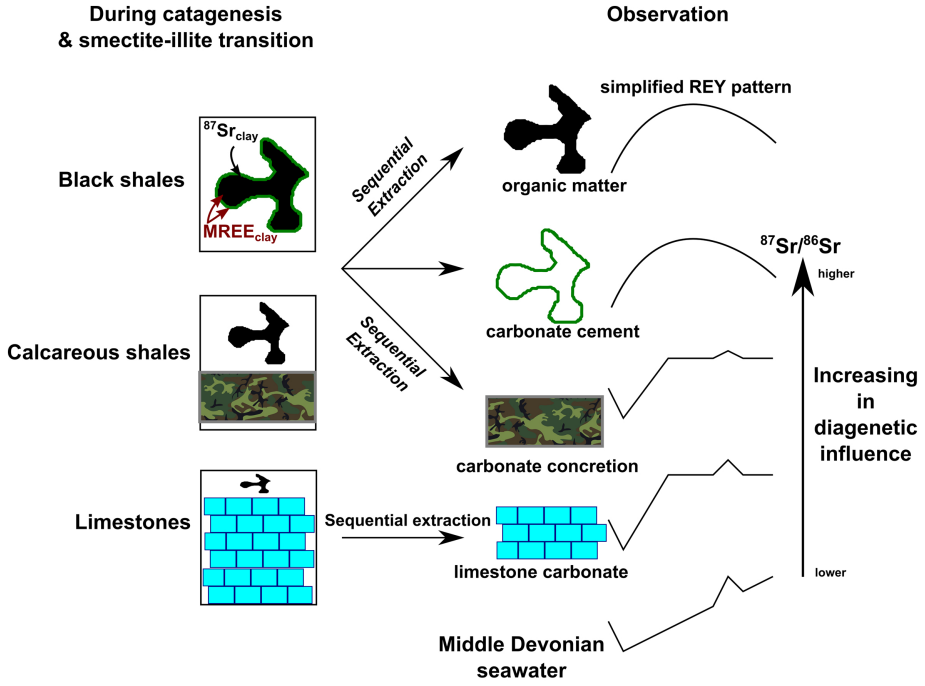

Carbonate Cements in Black Shales	**Carbonate Concretions in Calcareous Shales**
More significant diagenetic alteration	*Less diagenetic alteration*
Observations from this study	
MREE-enriched REY patterns More radiogenic $^{87}Sr/^{86}Sr$ that shows a good and negative correlation with sample depth No stratigraphic variation of Sr/Ca	Modern seawater-like REY patterns Higher concentration of REY relative to carbonate cements $^{87}Sr/^{86}Sr$ is close to unaltered Middle Devonian carbonates
Interpretation	
Expulsion of ^{87}Sr during smectite to illite transition REY released from smectite into pore fluid, then incorporated into remnant OM during catagenesis, REY signature later preserved in carbonate cement	Little evidence for diagenetic alteration

Figure 9